Current Opinion in Solid State and Materials Science 24 (2020) 100867

Contents lists available at ScienceDirect

Current Opinion in Solid State & Materials Science

journal homepage: www.elsevier.com/locate/cossms

Advances in fused deposition modeling of discontinuous fiber/polymer composites

Chao Hu, Qing-Hua Qin *

Research School of Electrical, Energy and Materials Engineering, Australian National University, Acton ACT, 2601, Australia

ARTICLE INFO

Keywords:
Hot melt extrusion
Fused deposition molding
Discontinuous fibers
Polymer composites
Multi-axis printing

ABSTRACT

Fused deposition modeling (FDM) is one of the most widely utilized additive manufacturing techniques by virtue of its numerous merits, such as easy operation, low cost, low energy consumption and little-to-no waste. Based on its simple configuration and extrusion-assisted process, the research and development of this technique is gradually shifting from traditional prototype printing to high-performance composite fabrication. This review provides a panorama for the recent progress of FDM technology in the manufacturing of discontinuous fiber reinforced thermoplastic composites. The entire production chain from the very beginning of FDM filament preparation to the latest stage in large-scale manufacturing process is discussed. The enlightening strategy in multi-axis FDM field is highlighted as it possesses a great potential to manufacture the next-generation composites with superior geometric complexity and flexible fiber alignment. This review also identifies the main challenges and outlook for the future development of this 3D printing technology in fiber reinforced composites.

1. Introduction

As one of the basic engineering materials, composites are composed of two or more constituents with utterly distinctive physical, mechanical and chemical properties. By organically integrating their different characteristics, these materials exhibit superior overall performance relative to their individual components [1–5]. Of all composite materials, the fiber reinforced polymer composites (FRPC) receives extensive research and industrial applications due to their exceptional strength to weight ratios [6–8]. To date, numerous techniques have been utilized in the manufacturing of FRPC like injection molding, compression molding, hand layup, resin transfer molding, filament winding, pultrusion and automate fiber placement [9–12]. Nevertheless, these conventional manufacturing methods require expensive molds, dies or lithographic masks and have the limitation for special fiber alignment, leading to the bottlenecks for the industrial production of complex and customized constructions [13]. Therefore, it becomes extremely imperative to explore new manufacturing technology to bypass long and costly processing procedures with more flexibility in structural design.

Additive manufacturing (AM), also known as 3D printing, rapid prototyping, or solid-freeform, is a disruptive technology that not only has a great potential to supplant many conventional manufacturing methods, but provide a new avenue for new products, new supply chains and new business services [14]. The fabrication process of a part through this technology is to add materials layer-by-layer directly manipulated by means of a 3D model, as opposite to subtractive methodologies. It starts with a meshed computer model that can be developed from the computer-aided design (CAD) software and converted into standard AM file formats that can be recognized by the corresponding 3D printers, such as surface tessellation language (STL) file or material template library (MTL) file. These files with sliced 2D layers can be further manipulated in terms of various machine-related processing parameters (e.g. infill density, infill pattern, layer height, wall thickness, etc.) to fulfil the part printing [15,16]. As a promising technology, AM offers distinct advantages over the aforementioned manufacturing methodologies. Designs for printed parts can be easily created, modified and shared so that the manufacturing process can be simultaneously carried out at different locations according to the client requirement [17]. Compared to the existing subtractive manufacturing (SM) processes that need to remove materials from their original blocks, AM makes the most use of raw materials to fabricate the final part by simply adding materials with minimal waste [18]. The fully customized parts with intricate geometries (internal or external) can be created in an economic manner without the use of additional machining tools (e.g. jigs, fixtures, cutting units, etc.). Studies show that this cost-effective technology is highly competitive to make the small lot-size (even one piece), for instance,

* Corresponding author.
E-mail address: qinghua.qin@anu.edu.au (Q.-H. Qin).

https://doi.org/10.1016/j.cossms.2020.100867
Received 19 June 2020; Received in revised form 30 August 2020; Accepted 4 September 2020
1359-0286/© 2020 Elsevier Ltd. All rights reserved.

with polymer injection molding for the targeted yield below 1000 items [19]. It, to a certain extent, facilitates the product design innovation by avoiding extra consideration of manufacturing and assembly principle [20]. Moreover, the lean production of maximum material utilization rate, low energy expenditure and minimal waste with recyclable and reusable residues endows AM with the capacity of designing and manufacturing environment-friendly products [21]. By altering material composition and topological structure within a part during the processing stage, gradient and multi-functionalities can be imputed into the printed product with hierarchical and multi-material features [22].

Since the AM concept was proposed from a patent by Charles Hull in 1984, multifarious 3D printing methods have been invented by encompassing a wide range of technologies [23]. According to the ASTM international standard F2792, all these AM techniques can be defined into seven categories of manufacturing processes in terms of their respective characteristics and limitations, including material extrusion, material jetting, binder jetting, sheet lamination, vat photo-polymerization, powder bed fusion and directed energy deposition [24]. By cause of the expired early patents regarding these AM methods and devices, a significant growth with annual average of around 30% is sustained after 2010 in global market sales (i.e. materials, products and services), mostly ascribing to the huge decrease for purchasing a commercial 3D printer with available price lower than $500 [25,26]. Industry is giving enormous investments in AM systems by perceiving the manufacturing advantages of these technologies including design improvement, assembly reduction through part consolidation and simplified production supply chains through point-of-use fabrication [27]. They have been witnessed the wide application in numerous fields, such as automotive and aerospace industries for complex and light-weight structures with high load-bearing capacities, biomedical and orthopedic industries for bioactive tissues, organs and implants, architectural field for prototype designs and electronic industry for active components [28–31]. In order to produce more than 100,000 3D printed parts for jet engines by 2020, General Electric sets the corporation plan of $3.5 billion investment in additive manufacturing [32]. The report from McKinsey Global Institute also estimated that the global economic impact caused by AM in 2025 will be $200 bn-$600 bn per year with the entire manufacturing cost reduction of 35%-60% [33].

Built upon the rapid evolution of various AM techniques, they have been flourishing in composite industry with the ability to incorporate various fillers into plastic printing. The manufacturing of FRPC via AM technology currently can be accomplished by the following 4 approaches: fused deposition modelling (FDM), selective laser sintering (SLS), laminated object manufacturing (LOM) and stereolithography (SLA) [11]. Among all these techniques, FDM is the most widely used and proliferated 3D printing process for FRPC fabrication by virtue of its cheap setup cost, low energy input and material consumption, minimal waste emission and facile operation [34]. Although the advancement of FDM technique in the past five years enables the 3D printing of continuous FRPC with its higher mechanical performance, the necessity for the modification of common 3D printers with complex processing makes it at the infant stage [35–40]. As the only company (i.e. Markforged) in the world successfully commercializing the FDM printer for continuous FRPC fabrication, most of the published researches are central in the employment of this machine with its monopolistic raw material supply, deficient matrix option (only one plastic material called Onyx), finite design freedom and extravagant cost [41–43]. It leads to a lack of robust and standard paradigm for the AM of continuous fiber reinforced composites. The mainstream for the FDM production of composite parts with intense investigation is still based on the application of discontinuous fibers as a filler due to relatively low cost, moderately improved mechanical properties and no machine modification requirement.

Dated back to the early 1930s, hot melt extrusion (HME) has been a well-established industrial manufacturing technology predominantly in the plastic processing, but also in food and pharmaceutical fields. The majority of polymer products involve HME in their manufacturing steps and the stage with HME processing typically accounts for 50% of the total energy expenditure [44]. As an independent machine, the hot-melted extruder can fabricate continuous sheets, tubes, pipes and FDM filaments while plastic parts like toys, spools, bottles, packages can be produced in association with other manufacturing techniques including injection molding, thermoforming and blow molding [45,46]. The basic principle of HME operation simply relies on the melting and cooling of thermoplastic polymers to form desired shapes, making it a green technology with solvent free trait [47]. Its unique blending geometry with highly customized screw configurations can promote high-shear localized mixing, contributing to the high-throughput manufacturing of composite materials with great phase uniformity [48]. The continuous operation with few processing requirements also endows this technique with higher scalability and time-/cost-efficiency [49].

In this review, an exhaustive overview is presented on the recent advances in the FDM manufacturing of discontinuous fiber reinforced composites (Fig. 1). As the indispensable upstream operation, the HME mechanism and its process for the fabrication of 3D printing filaments are at the first time summarized in a review paper. Then, the detailed FDM process involving material feeding, melting, extrusion, deposition and solidification is analyzed as well as the common composite feedstock involving various thermoplastic matrices, discontinuous fibers and support materials. Upscaling to an industrial level, the large-scale FDM system with higher productivity and larger build volume is also discussed. Furthermore, the state-of-the-art multi-axis FDM with higher design of freedom is highlighted as a promising technology to fulfil the manufacturing of topologically intricate FPRC. At the end of this paper, inspiring perspectives are concluded into future challenges and outlook for this specific field. Our review uniquely constructs a systematic

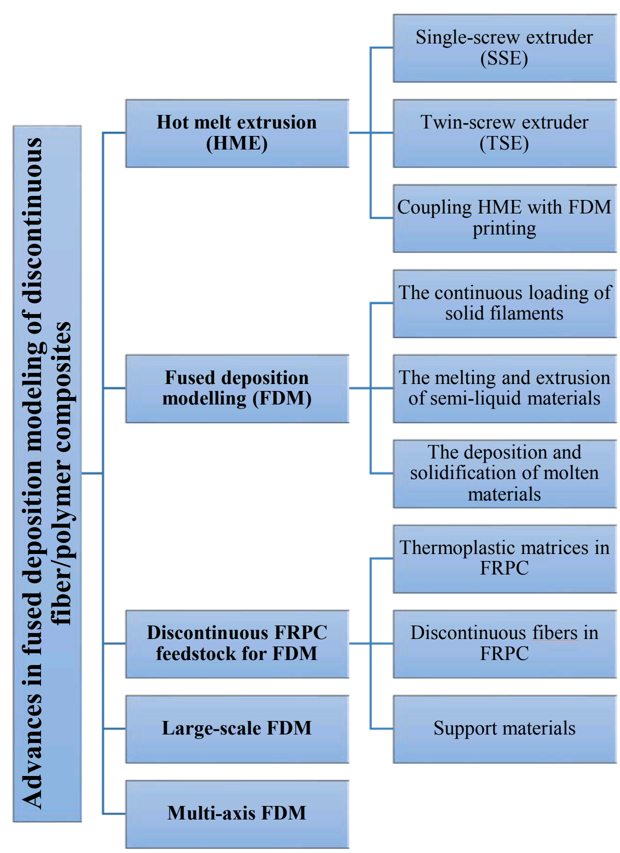

Fig. 1. Outline of the review. Flowchart showing the entire FDM system spanning from discontinuous FRPC material options, HME-based 3D filament preparation to the final FDM fabrication. The latest and potential technologies for the FDM-FRPC development are also discussed in this review.

knowledge spanning from the HME preparation of filaments, fiber/polymer material options to the evolution of various FDM processes. The summary of recent literature in this review will provide a series of cues to structure designers, engineers, material scientists and service suppliers to develop FDM-based fiber composites with better performance.

2. Hot melt extrusion (HME)

The HME system usually consists of an extruder, downstream processing equipment and other sensors to monitor and assess the product quality. The mixture of thermoplastic polymers and discontinuous fibers is added into the extruder through a feed hopper where the feed rate can be controlled by an electrically operated valve. The rotating screw located inside of the extruder barrel is driven by a motor so that the feedstock material can be conveyed at a predetermined speed. Concurrently, the polymer material is melted to mix with fibril fillers via multiple heaters in the barrel wall. Once the molten flow of material is pushed forward to the end of the barrel, a die is attached to assist the material extrusion into the desired shape. The extruded filament can be quickly cooled and solidified through a water tank, and then wrapped onto a spool via a collection unit. All these equipment and sensors are connected to a central control system in order to regulate the processing parameters such as barrel temperature, screw speed, feed rate, pressure, etc. More details regarding the operation and mechanisms of polymer based extrusion can be referred to the related reviews [50,51]. In recent years, HME has also be directly integrated with FDM into a single continuous process to achieve a more effective and efficient large-scale AM of FRPC (in section 6). Based on the material conveying mechanism, three types of HME can be defined: ram, single-screw and twin-screw extruders. Although the first type is easy by simply pushing the material with a piston, the discontinuous operation and inefficient heat transfer restrict its application [52]. Therefore, another two HME methods (i.e. single- and twin-screw extrusion) will be discussed in this section.

2.1. Single-screw extruder (SSE)

Invented in the 1870 s, SSE is the most widely used extruder by virtue of its simple operation in polymer and rubber processing [53]. The most fundamental configuration of SSE is the one rotating screw installed inside a stationary cylindrical barrel where three discrete zones can be distinctively subdivided: a feed zone, a compression zone and a metering zone [54]. Dissimilar pressures along the screw length can be generated based on the variation of the depth along with the pitch of screw flights within each zone. In order to consistently feed the materials from the hopper into the extruder barrel, the screw flight depth and pitch are normally designed at larger scales than those from other zones so that a very low pressure can be achieved at the feed zone. With the rotation-driven conveyance into the compression zone, the solid materials need to be melted and homogenized so that they can be converted into a suitable form to be delivered into the metering zone. Thus, a gradual increase of barrel pressure along the length of the compression zone is created by decreasing the screw pitch and/or flight depth [55]. Mixing, kneading and devolatilizing can also be accomplished in this processing zone for some less demanding applications [56,57]. With the stabilization of the effervescent flow into a steady state in the last zone (i.e. metering zone), a uniform product with consistent shape can be ensured from the die extrusion. Since it can produce a very high pressure during the operation, the manufacturing of extrusion-based products via SSE is extremely suited for highly viscous polymers [58].

The feed system for most SSE is flood fed via the extruder hopper, where the material is added through the feed throat into the barrel by gravitational force and the output rate is determined by the rotation speed of the screw. The high pressure generated in conveying materials from this feed system tends to compact the plastic pellets or powders into the solid bed [51,59]. Occasionally, the mass flow rate can be independent of the screw speed and regulated directly from the feed system based on the starve fed mechanism, leading to the output rate lower than the forwarding efficiency of the screw [60,61]. The occurrence of agglomeration can be avoided with the improvement of mixing action since the pressure accumulated along the screw is less than that from the flood feeding. The formation of a loose solid bed due to the much less compaction also facilitates the melting action as those polymer particles sustain their individuality [62]. However, the reduced capacity of extrusion throughput and more complicated operation with the introduction of a controllable feed device, to a certain extent, restrict the application of this feed system in SSE [63]. With the rotation of the screw in the extruder barrel, heat energy can be created owing to the friction between the rotating screw and the inner surface barrel. Combined with the heat flux from temperature-controlled heaters, the particulate materials can be melted from the solid bed into a viscous liquid pool so that the melted extrudate can be extruded out from the die for the further downstream processing [64].

2.2. Twin-screw extruder (TSE)

The SSE process is simple and cost-effective but does not possess a remarkable mixing capacity that is preferred for the manufacturing of polymer composites with multiple components compounded. Therefore, a modified extruder called TSE with two screws arranged side-by-side in the modular barrel was created in the late 1930s with the aim to form intimate mixtures of two or more materials [65]. In a typical TSE, the rotation of these two screws can be designed either in the same direction (co-rotating) or in the opposite direction (counter-rotating) (Fig. 2). Based on the positive displacement pump from the co-rotating twin-screw design, a wide range of mixing actions and efficient heat transfer are obtained with a faster throughput independent from the screw speed [66]. In contrast, the counter-rotating arrangement can produce a very high extensional shear force between the gap of two screws, enabling high pressure generation, potential air entrap, and long retention time with low screw speed and output [67,68]. Both of them can be further classified into fully intermeshing or non-intermeshing. As the most used type, the intermeshing TSE can not only reduce the non-motion during extrusion but avoid the localized overheat of raw materials due to its self-wiping feature. The rotation of both screws is able to remove residual materials from the screw roots and clean the whole inside barrel after the operation. Meanwhile, the product waste can also be minimized at the end of the production via this popular configuration [69]. For the non-intermeshing type, the mutually separate screws positioned in the extruder barrel result in a weak interaction and low torque generation, making it a better option in processing highly viscous materials and venting to remove internal volatile substances [70].

The diversity of screw designs also exhibits a wide variation of screw profiles in the same extruder with the intricate combination of two basic screw elements: conveying and kneading segments (Fig. 3). Also known as flighted segments, the conveying segments with relatively large channel depth (i.e. 2–3 mm for lab-scale extruders and several

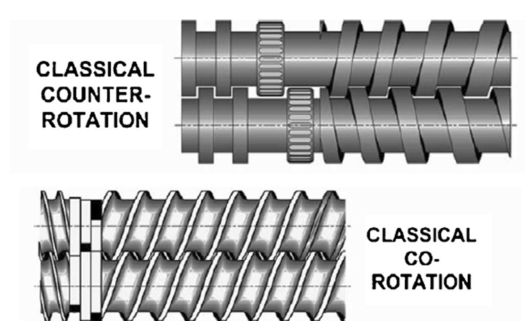

Fig. 2. The two types of screw design for twin-screw extrusion including counter-rotation and co-rotation [71].

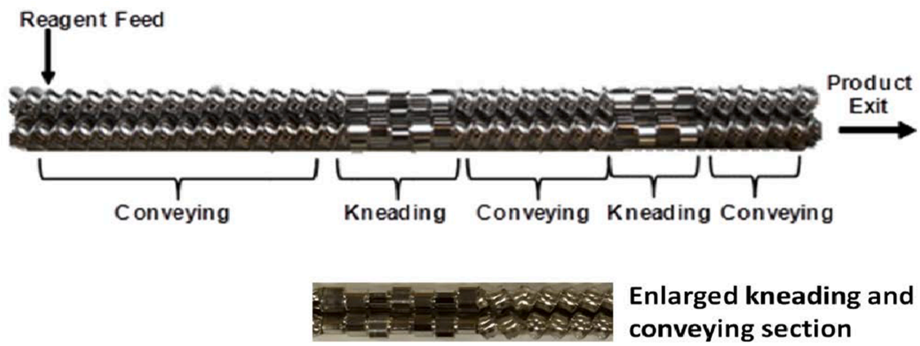

Fig. 3. The two basic screw elements in intermeshing co-rotating screws [72].

centimeters for industrial counterparts) are normally employed for the delivery of raw materials along the length of the extruder barrel. By modifying the pitch length and the amount of flights, the conveying rate in the feed and compression sections can be adjusted [72]. According to the difference of rotation directions in this element, the right-handed pitch ensure the consistent conveying of materials with high pumping capacity while the left-handed pitch (i.e. reverse screw segments) can yield intense shearing through pushing the molten material along the direction opposite to its flow towards the extruder end. The combination of these forward and reverse screw segments has been proved as an effective avenue to compress materials due to its great pressure build-up [73]. On the other hand, the kneading segments play a crucial role in mixing the different materials in the barrel. The kneading capacity can be regulated by positioning each of these segments at varying angles (e.g. 30°, 60° and 90°), and the last angle has the best homogenizing effect with the stagnation of these materials [74]. Although the kneading segments can provide a sufficient mixing action, they may also impair the material properties due to the excessive grinding force, such as the added fiber length and matrix rheology for the composite extrusion [75]. The modification of screw profiles by coordinating the arrangement of these screw segments endows TSE with greater versatility to achieve desirable shear, mixing and conveying levels. Meanwhile, it also well explains the large overlap existing in the processing capabilities of co-rotating and counter-rotating screw modes by virtue of the diversified design of screw profiles [76].

2.3. Coupling HME with FDM printing

Almost all thermoplastic-based materials used in the FDM process are prepared by HME in the form of continuous filaments. As an indispensable operation, how to manufacture good quality thermoplastic filaments from HME should be carefully concerned so that they can be successfully processed in FDM printing. The option of raw materials should be stiff yet flexible enough so that the produced filament from the extruder will not break during wrapping and unwrapping from a spool. To meet this requirement, a minimum strain at yield of around 5% has been recommended for its mechanical properties [77]. A sufficient strength and stiffness should be guaranteed so as to withstand the pushing and pinching force in the feeding mechanism of FDM. The constant delivery of a filament without buckling is essential to print a part with stable quality. Meanwhile, the filament fabricated from HME should have a proper viscosity to maintain the uniform deposition. A too low viscosity may lead to dripping while a too high viscosity could hamper the extrusion from the printing head, although higher nozzle temperature can be utilized to overcome this issue [78,79]. In addition, with the increase of fiber loadings and lengths, the continuous feeding of discontinuous fiber/matrix pellet mixture into the hopper of HME system is a big issue since relatively long fibers with high contents will gather at the feed throat to form a net-like structure, restricting the continuous adding of this mixture into the barrel. In one of our recently accepted patents, we invented an automatic material push-feeding setup that can be freely installed onto the feed hopper of the extruder. By punching the material throughout the feeding channel with varying rates, we eliminated the blockage of material flow at the throat and facilitated the homogeneous feeding of long fiber/polymer pellet mixtures into the extruder barrel [80]. Furthermore, high percentages of fibers may also increase the brittleness and cause the sharkskin instability for the HME-made composite filament, impairing the processability both in filament production and FDM printing [81].

3. Fused deposition modelling (FDM)

Invented by Scott Crump in 1989, FDM is the first commercialized AM technique through the founding of his company Stratasys and now holds the largest market in polymer based 3D printing [82,83]. Since FDM is trademarked by Stratasys at the beginning, this technique also has another equivalent term called "fused filament fabrication (FFF)", vividly depicting the fundamental mechanism underlying the melting and deposition of feedstocks in the form of filaments to print designed parts [84]. The basic structure of a FDM printer can be seen in Fig. 4. In general, the operation of a common FDM based system can be categorized into the following three steps: (1) the continuous loading of solid filaments via a feeding roller; (2) the melting and extrusion of semiliquid materials through a nozzle; and (3) the deposition and solidification of molten materials onto a build plate.

3.1. The continuous loading of solid filaments

The FDM process begins with loading the coiled filament from a spool through the feed system to the heated nozzle. It consists of two pinch rollers and a stepper motor where the stepper motor pushes the

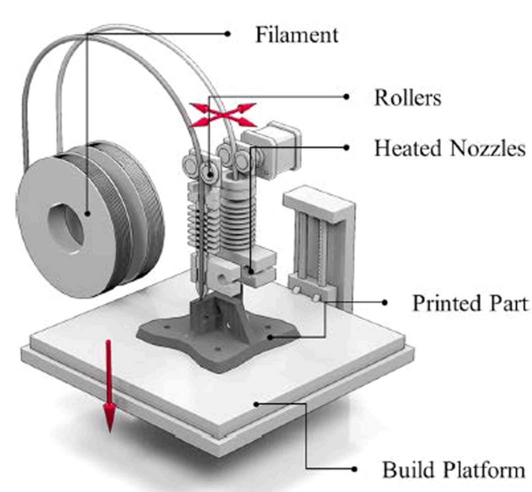

Fig. 4. The schematic of the basic structure for a FDM printer with red arrows showing the relative mechanical motion of components [84].

solid filament forward with the aid of a radial force exerted by pinch rollers. The surfaces of one or both of rollers possess grooved or toothed textures so as to avoid the slippage of the moving filament with sufficient friction [85]. To ensure a continuous and stable loading movement, a uniform and feedable filament with suitable mechanical and melt flow properties is required so that the constant amount of materials can be extruded for higher quality printing. By adopting a custom-made texture analyzer to simulate the forces of pinch rollers on the filament and map out the flexibility profiles from the recorded force-distance curve, Nasereddin et al. developed a simple mechanical screening approach to predict the feedability of a filament from the comparison of its profile with those of commercial counterparts via correlation analysis (Fig. 5) [86]. It is also crucial to minimize the deviation of the filament diameter since a big volume variation along the length causes errors in the printed shape. For instance, a thickness deviation of −0.25 mm in the filament may reduce the printed size by 11.29 mm^3 in a 10 mm material consumption, which corresponds to 15.98% of the nominal volume [87]. The HME manufactured thermoplastic based filaments for FDM normally have three thread diameters: 1.75 mm, 2.85 mm and 3 mm [88]. For the thicker filament, its high strength and stiffness promote a smoother loading process with less likelihood of filament breakage from the large compression force of rollers while more pressure is needed to push the material into the nozzle. In contrast, the thinner filament can be fed easier and faster through the same nozzle size but its high flexibility may result in buckling and twisting through the curved guide tube during the material loading [89]. No matter which diameter is selected in FDM process, the printed parts can be maintained with similar qualities once the processing parameters are fine-tuned.

In situations where the filament is too brittle, humid or inhomogeneous (sustaining inconsistent pushing force), fracture may occur during the material feeding with the discontinuity for the forward thrust of the filament, causing the jam in the guide tube or clogging in the printing head. This severe issue can not only contaminate the printer with the material burning at the heated nozzle, but bring about geometrical misalignments or failure of the printed part [90]. Since there is no solution currently able to deal with this problem automatically in FDM machines, operators need to visually identify it, manually terminate the printing, clean the feeding system by disassembling the entire printing head and restart the whole part from the scratch [91,92]. Thus, the monitoring of filament breakage in the material loading plays an important role in guaranteeing the successful FDM operation. By introducing an acoustic emission (AE) sensor into the loading system, Wu et al. created a lightweight FDM machine condition monitoring tool to identify both normal and abnormal printing states. As AE hits, the original waveform signals were received and simplified via the combined application of principle component analysis and the hidden semi-Markov model so that common machine failures like the material run-out or filament breakage can be diagnosed in a real-time fashion [93]. Based on the same AE technique, Yang et al. deduced the different probability distributions of AE signals by employing two quantified indicators (i.e. instantaneous skewness and relative similarity) to accurately identify the filament breakage from the steady feeding state, offering a potential strategy for in situ loading detection of FDM process [94]. The optoelectronic contact switch or mechanical contact switch are also utilized in industry to monitor the breakage while these methods can only detect the existence of material in the channel. They are incapable of identifying the dynamic motion of the filament, restraining the effective diagnosis in material loadings.

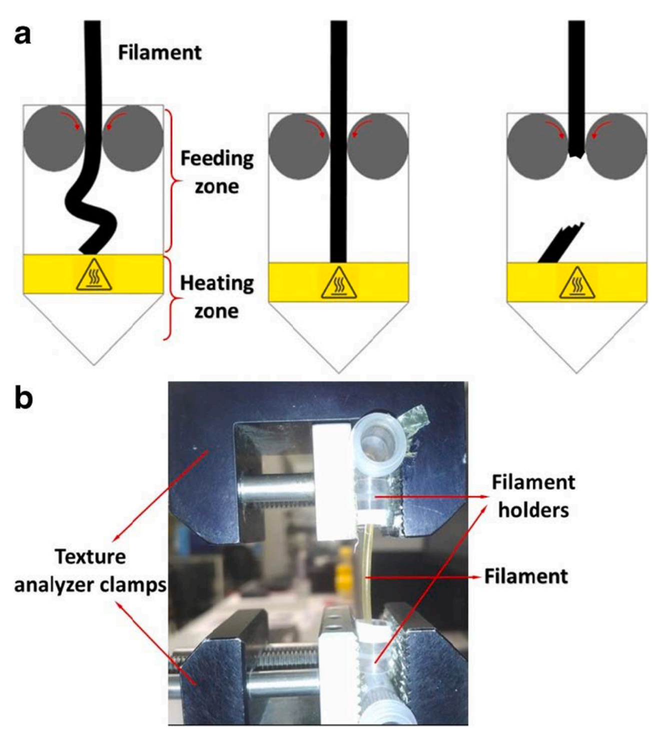

Fig. 5. The filament loading via pinch rollers in the feed system: (a) different behaviors of loaded filaments including buckling, stable feeding and fracture; (b) the rest rig for the texture analysis of filament feedablility [86].

Improvement in the throughput of FDM process is essential to fulfil the vision of maximizing the machine utilization and advancing the production efficiency with less lead time. One critical strategy is to increase the build rate via the printing head. Both of current desktop and professional FDM machines have the similar rate (∼10–100 cm^3/h) in part printing, though the latter is more remarkable in maintaining dimensional accuracy and overall quality [95]. This relatively slow build rate can be attributed to the limitations of three key modules in a FDM system: the maximum traction force of rollers from the material feed mechanism, the heat transfer rate from the thermistor to the filament core in the liquefier, and the moving speed of the printing head positioned in the gantry. Of all, the complex regulation of the feed rate is not only restricted by the pressure drop in the liquefier, but affected via the trade-off between the maximum traction of feed rollers and filament facture [85]. Through the FEA simulation of technical parameters in the modules of several commercial printers, Go et al. analyzed the rate-limiting mechanism and mapped a unifying trade-space of volumetric build rate versus resolution as a function of extrusion force, liquefying temperature and gantry speed, predicting the big possibility in enhancement of FDM build rate via the optimization of these modules (Fig. 6) [95]. In consequence, a "FastFFF" system was developed, in which a rotating nut was adopted in the feed device so that a faster feed rate can be achieved. Combined with a laser-heated liquefier and servo-driven parallel gantry, the maximum extrusion rate and volumetric build rate in this prototype system respectively reached at 282 cm^3/h and 127 cm^3/h, which were ∼ 14-fold and ∼ 7-fold greater than commercial FDM printers (Fig. 7) [96]. This system as an example overcomes the module-level performance constraints and offers a promising potential to adapt into the high-speed printing of fiber-filled composites.

3.2. The melting and extrusion of semi-liquid materials

As the pivotal operation of a FDM system, the thermal process that takes place at the liquefier plays a vital role in regulating the melting and extrusion of semi-liquid thermoplastic-based materials. During this process, the input filament is loaded forward into the liquefier body where the solid material experiences a progressive heating up until its glass transition temperature (T_g) is surpassed [97]. The heat flux received by the filament converts the physical state into a thick semi-liquid material, allowing it to be extruded out from the print nozzle at the end of the liquefier. In order to ensure a continuous and stable material flow without blocking the tip of the nozzle, the temperature at the nozzle must be kept constant, which is achieved by the coiled

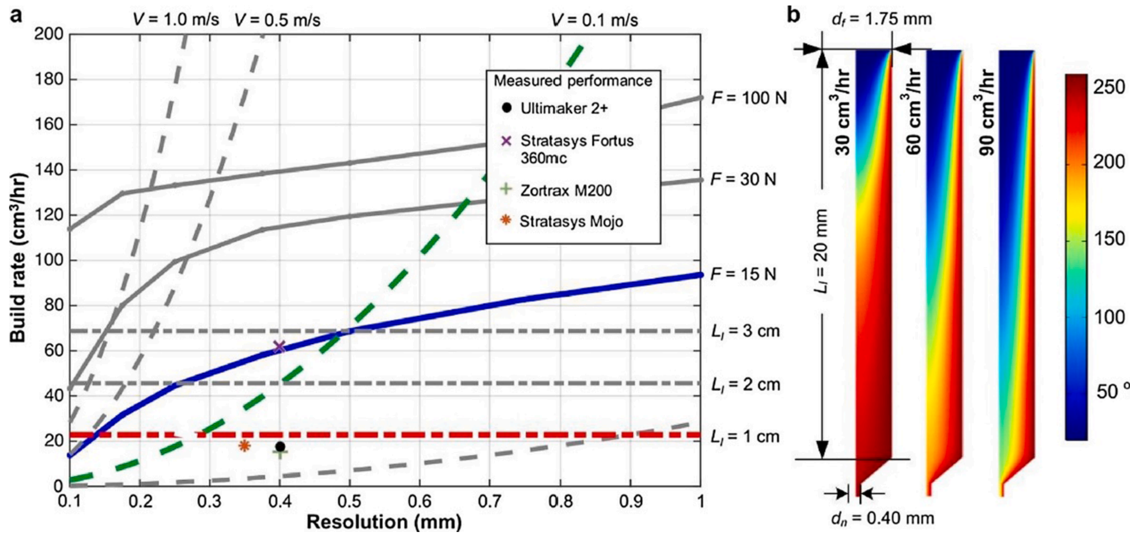

Fig. 6. The performance summary of conventional FDM system: (a) the trade-space of volumetric build rate versus resolution in several desktop FDM printers that is constrained by maximum traction force of rollers, heat transfer rate in the liquefier and moving speed of the printing head. The common area under three curves is the accessible performance from these selected commercial FDM printers; (b) the temperature distribution in a liquefier at varying volumetric rates, indicating the limited heat penetration at higher feed rates [95].

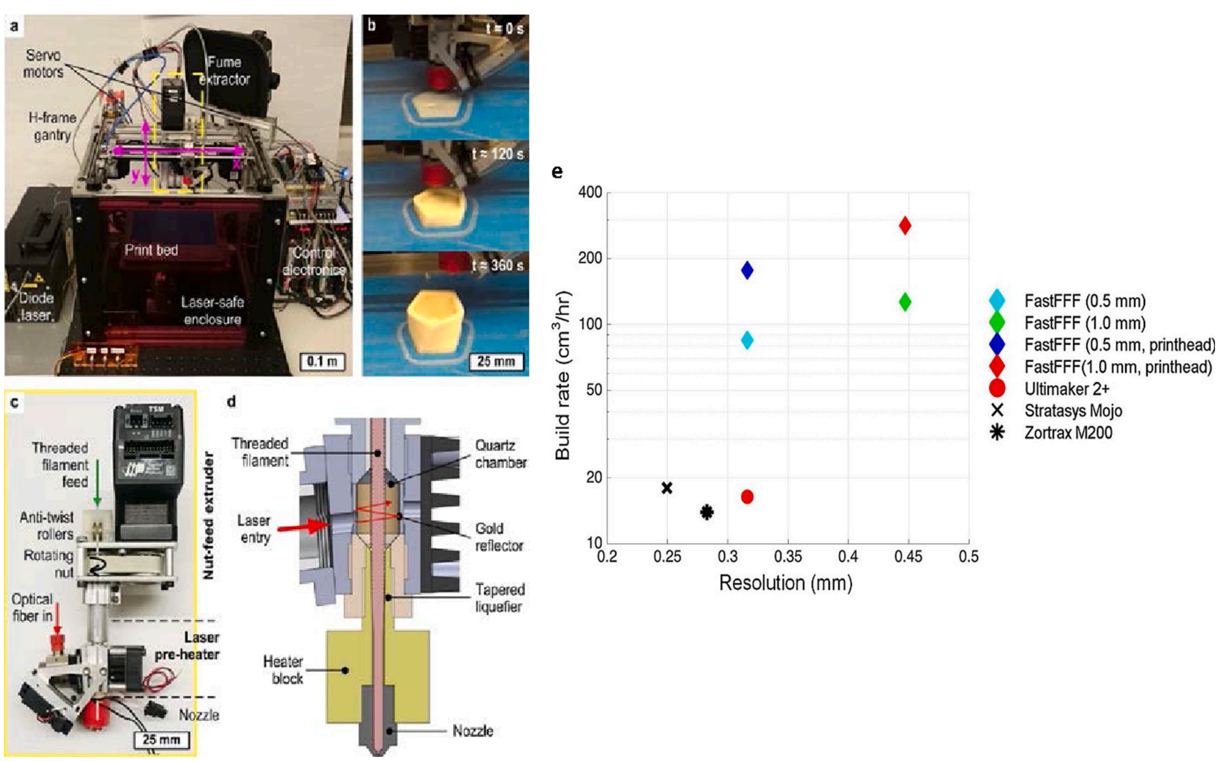

Fig. 7. The FastFFF system with high-throughput printing head design: (a) the desktop FastFFF printer with H-frame gantry, diode laser with fiber coupling to printhead, and control electronics at a build volume of 185 × 125 × 200 mm; (b) photos for the printing of a spiral cup as a function of time; (c) photos for the nut-feed drive unit and laster-assisted heater in the printing head; (d) cutaway solid model of the liquefier, showing how laser is coupled to filament as it travels through a quartz chamber surrounded by a reflective gold foil; (e) the comparison between FastFFF system and commercial destop FDM systems in terms of volumetric build rate versus resolution [96].

resistance heater or cartridge heater inside a heat block. Besides the heating element, the heat block attached at the top of the nozzle also houses a thermistor (i.e. temperature sensor) to control and monitor the required temperature for the specific printed material [98]. Although the solid material inside the nozzle must be heated to an objective temperature for melting, the upper part of the filament should remain as cool as possible to avoid the possible jamming. Therefore, a heat barrier made of a low conductive stainless steel joins at the top of the heat block to reduce the upward heat conduction. In fact, minimizing the upward heat flow from the heat block can not only save more energy to maintain the desired temperature by preventing the heat lost and shortening the working time of resistance heater, but avert the discontinuous flow of the material due to the frequent fluctuation of temperature [99]. In order to further decrease the temperature close to the ambient environment, a heat sink composed of a finned case with an external cooling fan is connected with the heat barrier to dissipate heat via convection (Fig. 8). This is necessary to protect the hardware durability since supporting elements that fix the heated liquefier body to the gantry are made from common plastics (with low weakening temperatures) and could be subjected to irreversible deformation or failure at the prolonged overtemperature, leading to the mechanical dysfunction of the printing machine [100].

The design and functionality of a nozzle in a standard FDM liquefier are extremely important to govern the accuracy, productivity and build quality of printed parts. One of the biggest determinants for the performance of the nozzle is the orifice size. Typically, the diameters of printing nozzles range from 0.1 to 1 mm so that the ratio of the maximum diameter contraction of the filament to its original thickness can ascend to 1:30 [102]. However, the most widely used nozzle size for a desktop FDM printer is 0.4 mm (e.g. Ultimaker 3 and Makerbot Replicator) since this size is small enough to achieve a refined surface quality of parts and maintain a reasonable build time [103]. It should be noted that the layer height should never be larger than the nozzle size because the bonding strength between neighbouring layers will be drastically decreased. This can be attributed to the reduction of contact area between the extruded layer and the previous deposited layer, thus leading to their insufficient mutual bonding. For the sake of increasing the deposition rate and build volume to meet the requirement of industrial manufacturing, the large-scale FDM system employs the nozzle with much large sizes while the print resolution and surface finish are usually compromised. Post-possessing methods like polishing and coating must be added to eliminate the rough surface of parts, which will be more time consuming and labor intensive than the initial printing. Recently, Chesser et al. created a novel nozzle-selectable system and integrated into the large-scale FDM liquefier, where the nozzle size can be altered mid-printing by utilizing a poppet nozzle selector (Fig. 9.). With this system, the interior of a part can be printed at a course resolution by using a large nozzle size while the surface can be fabricated at a fine resolution by shifting to a small nozzle diameter. The results from this work demonstrated that compared to the interior resolution of the composite part, a doubling of exterior resolution can be achieved without a significant increase of printing time [104]. As a new selective resolution printing technique, more work needs to be done to explore its industrialization potential, such as using finer nozzles for critical areas and developing relevant software algorithms for the intelligent selection of improved surfaces.

The thermal dynamics and pressure gradients in the FDM liquefier play a critical influence on the viscous flow of the material and the subsequent deposition onto the build plate. It has been demonstrated that a proper melt temperature can decrease the flow viscosity and facilitate the mutual bonding of extruded beads while a too high temperature may degrade the material by damaging inner polymer chains. If the temperature is too low, the insufficient melting of the solid material with low pressure drop could also give rise to filament buckling [105].

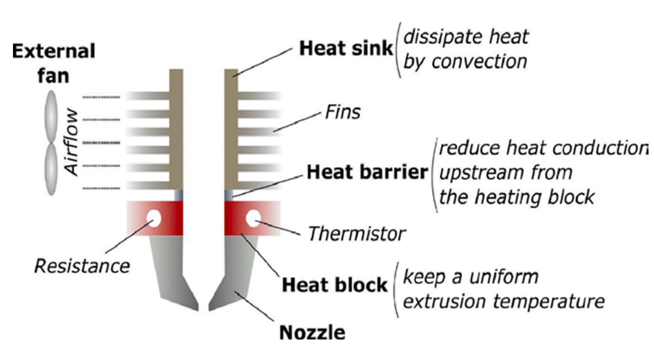

Fig. 8. The general structure of a standard FDM liquefier with all functional parts [101].

Many scholars conducted the theoretical research to understand the thermal history and behaviour of the material melting and extrusion in the liquefier [106–108]. For instance, Bellini et al. investigated the transfer function of a liquefier through a mathematical model and found a strong dependency of the material viscosity on the nozzle heating [109]. As a significant factor affecting the bio-scaffold quality, Ramanath et al. studied the melt flow behaviour of poly-ε-caprolactone in a liquefier of a FDM printer via using two methods: mathematical modelling and finite element analysis (FEA) via Ansys®. The comparative results from these two modes revealed that the variation of nozzle diameters (0.25–0.4 mm) and angles (20-60°) has a direct impact on the pressure drop along the melt flow channel. The temperature gradient analysis shows the solid biopolymer was liquefied within 35% of the channel length [110]. Yardimci et al. presented a 2D deposition thermal model by utilizing corresponding analytical and computational thermal design tools to quantify the effect of nozzle design on the operational stability and temperature distribution near the vicinity of extrusion point [111]. Different from most studies focusing on the position of the melt front, Jerez-Mesa and his team designed a FEA model to tackle with the convective heat dissipation along the heat sink of a BCNozzle liquefier by the refrigerating fan. The predicted temperature profiles from the model with varying airflow velocities were validated with discrete temperature values measured via four thermocouples fixed on the liquefier body, confirming its adequacy to be applied for other working conditions [112]. Further exploration on the impact of overheat along the heat sink will also be useful to correlate the maximum acceptable temperature with the fan working regime for more energy saving. Considering the lack of related studies regarding the internal geometry of a liquefier on thermal behaviour of FDM system, the same group compared one commercial liquefier with two customized variations by adopting the same theoretical and experimental methodologies. Results show that the new design of a thick-fin heat sink with higher structural simplicity has the best performance of 3D printing under a fan velocity higher than 10% and a much lower manufacturing time than the commercial counterpart [101]. Without doubt, this work provides some insight into the heat transfer effectiveness of a certain liquefier and the optimization of this printer core component with more stable and precise temperature control.

With respect to the melting and extrusion of FRPC, the great importance of thermal dynamics in FDM liquefiers as a function of their structures and interaction between parts is also projected onto the fiber orientation in the melt flow. With the application of the Moldflow injection molding analysis package, Nixon et al. modeled the fiber orientation in the extruded beads from three different nozzle designs (i.e. convergent, divergent and straight geometries) in the FDM system. The largest overall fiber alignment was observed in the convergent nozzle while the divergent nozzle exhibited the least fiber alignment. However, before entering into the nozzles, fibers in the flow were oriented uniformly in all three liquefier channels [113]. Heller et al. presented a computational method to analyze the effects of nozzle geometry and extrudate swell on the fiber orientation in the polymer melt flow. The authors demonstrated a great fiber alignment along the flow axis within the convergent zone of the nozzle while a decreasing trend was observed in the extrudate swell, leading to a 19.9% reduction in the axial modulus of elasticity. By varying nozzle parameters, this study indicates the possibility of regulating the fiber orientation and mechanical properties of printed FRPC via the modification of FDM nozzle geometry [114]. Inspired by complex fiber arrangements in natural composites, Raney et al. developed a rotational 3D printing system with a controllably rotated deposition nozzle that enabled the spatially programmable orientation of short fibers in the polymer matrix (Fig. 10.). With the variation of rotation speeds, these researchers incorporated two fiber patterns (i.e. orthogonally and helically arranged fibers) into different sections of the printed composites, presenting high microstructural complexity and enhanced performance in strain, failure and damage tolerance [115]. In short, the specific design of a liquefier body has a

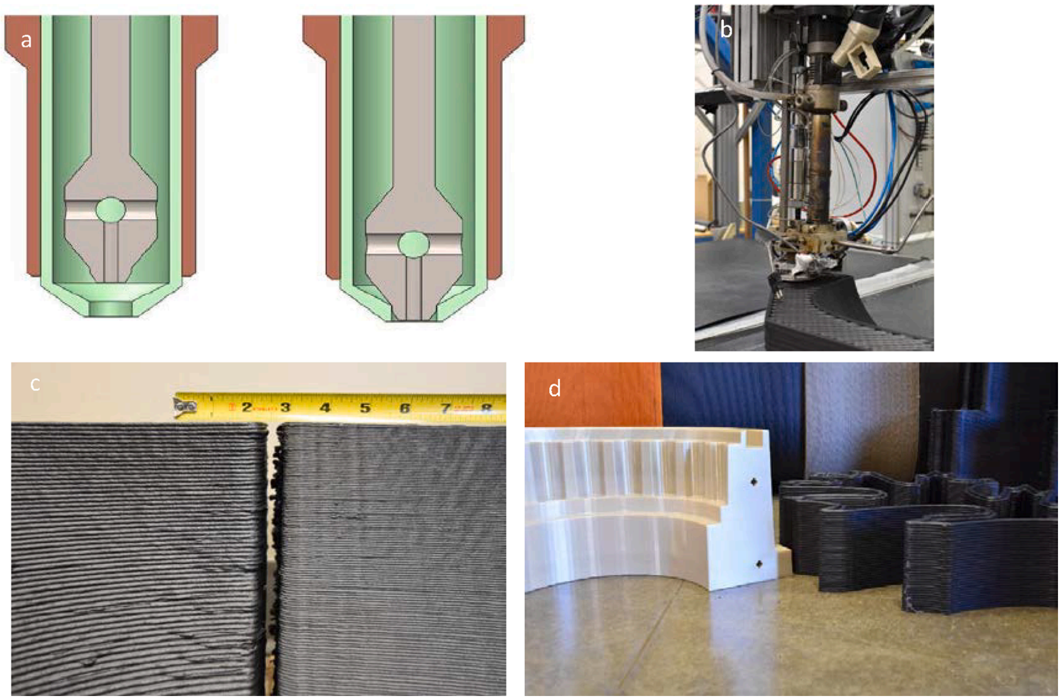

Fig. 9. FDM printing of fiber composites with varying resolutions via selectable nozzles: (a) the poppet selector in nozzle to adjust size; (b) the fiber composite printing with multi-diameter nozzle; (c) close-up comparison of surface resolutions between normal nozzle and diameter-selectable nozzle in large-scale FDM system; (d) the printed part comparison between small-scale and large-scale FDM systems [104].

crucial influence on the fiber orientation in the printed bead while the fiber orientation can also affect the flow field during extrusion. Due to the computational complexity for anisotropic flow, the currently limited researches simplify the modeling to consider fiber/polymer system as Newtonian isotropic fluids, which cannot accurately reflect the fiber orientation state [116]. Hence, more advanced simulation tools integrated with supercomputing are in demand for the precise prediction of the flow field and fiber orientation in the extrusion stage of fiber composites.

The measurement and monitoring for the temperature and pressure of the filament during the extrusion are vital to obtain a consistent part quality since any fluctuations in these conditions may produce significant impacts on the material flow, deposition rate and intra-/inter-layer bonding. As to the vast majority of FDM printers, the localized temperature is the only information that can be collected through a single thermistor located at one side of the heat block. To interpret its variation throughout this print head, the employment of multiple thermistors by some solvers can be an approach but higher probability of fluctuations is still a big issue [117]. Although infrared cameras can be integrated into the liquefier body to monitor the temperature, the observation from these devices is confined to the surface of the nozzle [118]. None of these measurements can determine the temperature variation inside the semi-liquid filament as the sensors are not in direct contact with the flow. In addition, almost all the pressure measurements inside the liquefier are inferred from mathematical modelling and FEA due to the big technical challenge in the small nozzle channel. Only one report currently enables the in-situ measurement for these two processing parameters in the melt. By creating a customized thermocouple insertion device coupled with a piezoresistive pressure transducer, Anderegg et al. successfully recorded the temperature and pressure distributions in the flow field during extrusion. Readings showed the fluctuation of $\pm$ 2 °C and up to 11 °C decrease in filament temperatures respectively at idle and at high flow rate. There was also a significant fluctuation in pressure (140–6900 kPa) and the in-situ measurements were higher than theoretical predictions, indicating the limitation of computational modeling to completely capture the dynamics in the FDM liquefier [119]. Aside from the improvement of the internal process monitoring, this system also provides an empirical avenue to investigate the mutual relationship of various variables in FDM, including the flow rate, rheology, heat transfer, pressure drop, nozzle geometry and filler distribution.

3.3. The deposition and solidification of molten materials

In a typical FDM, the printing head installed onto a gantry is movable along X, Y and Z axes so that the deposition of material can be initiated from the nozzle by its horizontal translation at a constant height over the build plate. After the first layer, the succeeding layer is deposited via either the ascent of the printed head or the descent of the build plate, which is dependent of the individual printer [120]. This automatic process for each layer printing is repeated until the completion of the designed part. During this deposition and solidification process, the cross-bonding between beads is established by the inherent thermal energy of the extruded semi-liquid filament. A bridge between the adjacent beads called a neck is formed due to the sintering process driven by surface tension (Fig. 11). Different with metal and ceramic sintering governed by volume, surface and grain boundary diffusion, the polymer sintering describes the coalescence process below the melting point based on the viscous flow mechanism [121,122]. The mutual bonding of beads with neck growth within a layer can be termed as intralayer bonding. Meanwhile, as the bead from the next layer deposits over the previous layer, its high temperature also facilitates the formation of similar bonds between the beads of two successive layers, which can be termed as interlayer bonding [123]. Consequently, the printed objects by conventional FDM system are normally anisotropic whether in topological geometry or in physical properties.

The extent of bonding lies with the neck growth between the beads and the molecular diffusion and randomization of polymer chains at the interface. Combined with the isothermal sintering experiment, Bellehumeur et al. utilized the polymer sintering model to predict the degree of bonding during the deposition in FDM. Results showed that the neck growth in the bonding zone was more affected by the extrusion temperature rather than the envelop temperature [125]. On the contrary,

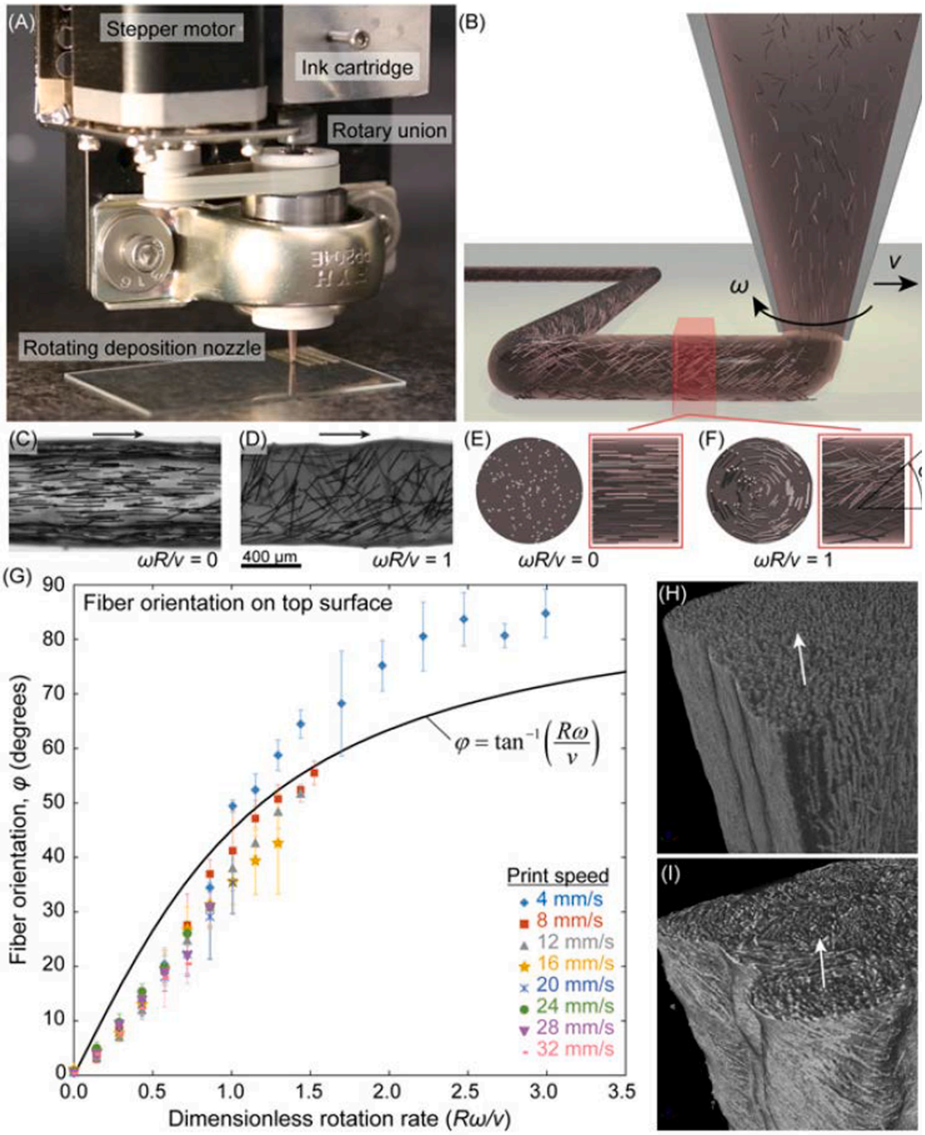

Fig. 10. The rotational 3D printing system: (A) the controllable rotation of the nozzle during printing conducted by directly interfacing a stepper motor with a 3D motion-control system; (B) Schematic view of fiber orientations via the rotating nozzle to obtain a helical pattern, where the helical angle is adjustable by the rotational rate (ω) and translational velocity (v); (C and D) Optical micrographs of fiber-filled composite filaments (1.3 vol% carbon fibers) printed without rotation and with a high rotation rate; (E and F) schematic views of idealized fiber arrangements for the same dimensionless rotation rates; (G) Surface fiber orientation (φ) plotted as a function of dimensionless rotation rate (Rω/v) over a wide range of rotational and translational rates, where the solid line denotes the kinematically ideal fiber orientation; (H and I) Cross-sectional views of the internal structure of composites printed without rotation and with a high rotation rate, observed by X-ray microtomography (print direction indicated by arrow) [115].

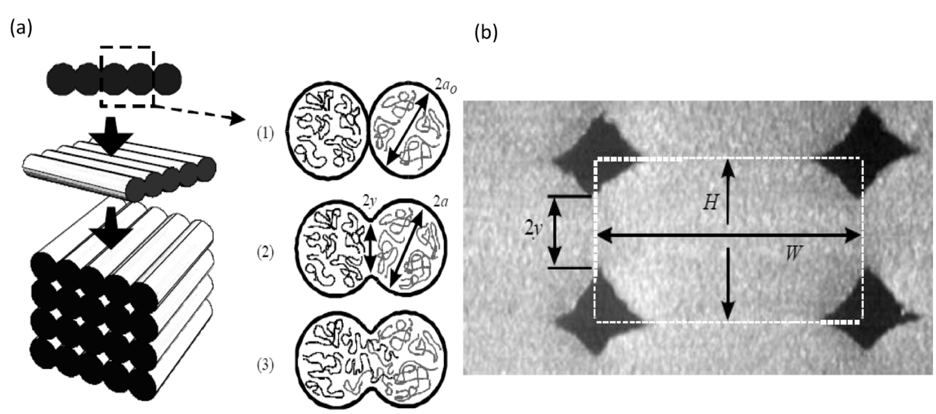

Fig. 11. Bond formation between adjacent beads in FDM process: (a) the schematic of bond formation process involving (1) surface contacting, (2) neck growth and (3) molecular diffusion at interface and randomization; (b) the microphotograph of the cross-sectional area of a FDM part where W is the filament's width; H is the filament's height; 2y is the neck length between adjacent filaments [124].

Sun et al. found that both the envelope temperature and variations of convective coefficients within the printer chamber have a significant impact on the mesostructured and mutual bonding of beads via the characterization of flexural properties. The sintering process also has a great repercussion on the bond formation while the critical temperature cannot be maintained too long above the glass transition owing to the fast cooling of the extruded filament [124]. Bhalodi and his team observed that the temperature at the neck between two neighbouring beads decreased exponentially with time through relating time and temperature in a mathematical model [126]. This short sintering process has been validated as the main reason for the imperfect bonding of partial coalescence, resulting in the generation of voids between each bead [127]. Numerous reports have concluded that the insufficient bond with voids acting as stress concentrators has a negative influence on the mechanical performance of the 3D printed parts, especially for the weak interlayer strength along the Z direction [128–131]. To address this issue, Ravi et al. integrated an in-process near-IR heating laser into the 3D printer to locally heat up the existing layer around the nozzle before the deposition of the extruded bead at this heated area (Fig. 12). The increased interpenetrating diffusion from the raised interlayer temperature contributes to 50% more interlayer bonding strength, 60% increase in bending strength, near 100% increase of elasticity and more than triple toughness of the FDM part compared to the counterpart without laser pre-deposition heating [132]. With the addition of 2 wt% thermally expandable microspheres in the polymer matrix, Wang et al. reported a material-based approach to improve the interlaminar bonding with reduced voids via heat treatment after FDM fabrication. Compared to untreated samples, the tensile strength and compressive strength were respectively increased by 25.4% and 42.2% after keeping them at 140 °C for 120 s [133]. Besides the presence of voids, Rodriguez et al. discovered that the loss of molecular orientation after deposition was also an important factor in the decrease of overall mechanical properties in FDM parts [134].

The sequential deposition of fused material layers involves the cooling by convection into surrounding air and the solidification onto the previous layer via heat conduction through the adjacent bead [135]. These rapid cooling cycles exacerbate the non-uniform thermal gradient with irregular heat distribution throughout the printed structure, resulting in the build-up of internal stresses within the deposited layers. A bunch of problems have been caused in the final part by the thermal-induced residual stresses and strains, including dimensional inaccuracy, shrinkage, warping, delamination and even printing failure [136,137]. For instance, Wang et al constructed a mathematical model for the warp deformation, in which the T_g and linear shrinkage rate have been demonstrated as influencing factors for the appearance of intra-/inter-layer deformation, delamination and cracking [138]. Zhang and Chou developed a 3D model with the introduction of additive feature and stepwise thermomechanical manner to simulate stress distributions and part distortions as a function of several deposition parameters. Results showed that the residual stress was significantly affected by the scan speed followed by the layer thickness while the influence of the road width on the stress accumulation was only effective under the interaction with the layer thickness. The positive correlation between part distortions and these deposition parameters derived from this model has a great consistence with the deflection experiment [139]. Assisted by the FEA analysis and element activations, they also found that the toolpath patterns played an important impact on both the magnitude and distribution of residual stresses, in which the primary direction of the designed toolpath guided the stress concentrations. From that simulation, higher residual stresses and larger distortions were observed in short-raster toolpath than those in long- and alternate-raster patterns [140]. Via embedding a fiber Bragg rating sensor into the midplane of FDM samples, Kantaros and Karalekas experimentally verified the sensitivity of residual strains to the deposition orientation in the in-situ solidification test, recording less strains for the beads aligned to the 0° direction than those in transverse and crisscross counterparts [141]. Armillotta et al. studied the influence of part geometries on warpage and found less distortion on very thin parts, which is contradictory to other literature suggesting that a lower z-direction dimension results in lower bending stiffness and thus large warpage. Based on a 1D analytic model, they proposed a different interpretation that a thinner part height can not only facilitate the shrinkage on multiple layers via thermal conduction and contribute to the reduction of internal stresses, but cause plastic deformation of the deposited layers to keep flat on the build plate under bending stresses, opposite to the occurrence of elastic deformation in thicker object that will be recovered as distortion [142].

According to the above discussion, it is perceptible that considerable variables are involved into the fabrication process of this simple AM technology, including the part geometry (e.g. length, width, height, spatial structures, etc.), material properties (e.g. strength, modulus, Poisson's ratio, T_g, etc.) and processing parameters (e.g. layer thickness, deposition rate, nozzle temperature, chamber temperature, raster angle, bead orientation, number of contours, etc.) [143–145]. The analysis of all these interactive variables cannot be isolated, further increasing the complexity to assess the possible influence of individual factor on the FDM part quality. Last year, the material database 3D-printing grades from DSM was integrated into the FFF process simulation software Digimat, becoming the first commercial modelling tool for AM engineers

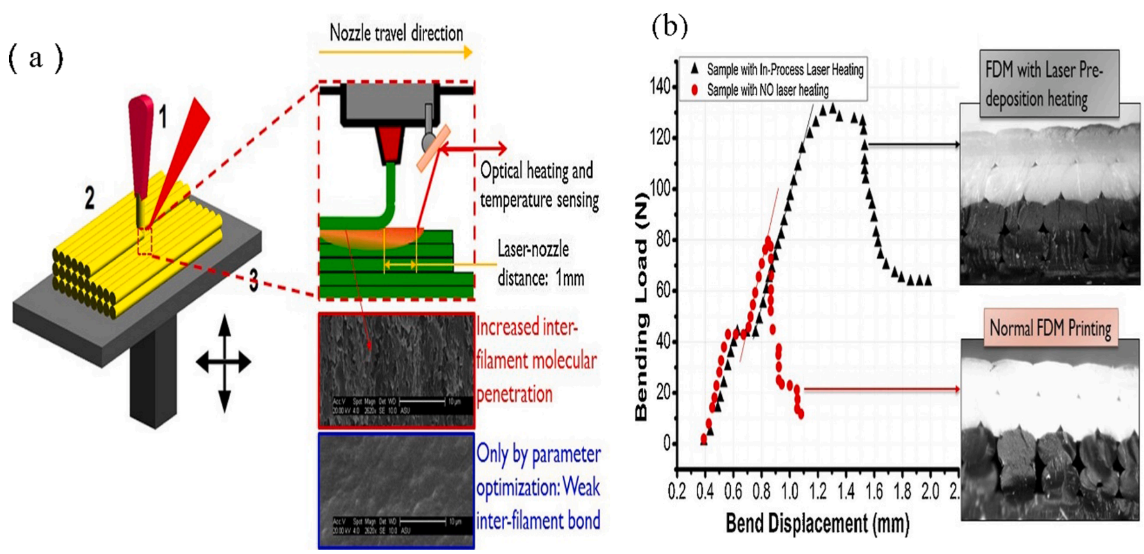

Fig. 12. The integrated laser pre-heating system to enhance the inter-layer bonding in FDM: (a) the layer fixed ahead of the printing nozzle so that the previous deposited layer can be heat up with higher interface temperatures to allow more polymer inter-diffusion between neighbouring layers; (b) the flexural results show that the laser pre-heated samples had more than 60% increase of strength, around 100% increase of elasticity and more than 3-fold toughness compared to the FDM counterparts without laser treatment. Micrographs demonstrate enhanced filling, contributing to overall better mechanical performance in printed parts [132].

to predict the behaviour and performance of printed parts so that the optimization of materials, printers and designed geometries can be realized [146]. However, the options in this database are still limited to some basic materials without a good cover for composites.

4. Discontinuous FRPC feedstock for FDM

4.1. Thermoplastic matrices in FRPC

As it was mentioned above, both of HME and FDM processes are built upon the melting and cooling of materials to obtain the desired shape. In a sense, the extrusion-based FDM technology can be deemed as the automatic upgrade of the conventional HME method. Thus, the reversible liquid–solid state change of thermoplastics makes these polymers to be the eligible feedstock for these two manufacturing techniques. Compared to thermosetting resins, these heat-regulated polymers alone or as composite matrices have numerous unique merits, including high recyclability, less hazardous chemical compositions, no curing requirement and ease of mass production [147]. The common thermoplastic polymers that can be utilized as composite matrices for FDM process include acrylonitrile butadiene styrene (ABS), polylactic acid (PLA), high density polyethylene (HDPE), polypropylene (PP), polyamide/nylon (PA), polycarbonate (PC), thermoplastic polyurethane (TPU), polycaprolactone (PCL) and polyethylene terephthalate (PET) [148–151]. The commercially available polymer filaments in the FDM market can be seen in Fig. 13 [152].Among them, ABS and PLA are the most extensively used 3D printing thermoplastic. The former is a tough terpolymer composed of a long polybutadiene chain criss-crossed by short chains of poly (styrene-co-acrylonitrile) and can be printed at high speed while it tends to warp and delaminate when printing large parts. The latter is a biodegradable and biocompatible aliphatic polyester derived from renewable resources (e.g. corn and sugarcane) and harder than PLA. Although it can strongly adhere to the build plate without the need of heating, this polymer is prone to jam in the liquefier owing to its high friction [153]. Other expensive engineering thermoplastics (e.g. poly ether ether ketone (PEEK), poly ether ketone ketone (PEKK), polyphenylene sulphide (PPS) and polyeherimide (PEI)) with higher thermal and mechanical performance can also be printed while specialized AM machines are required, further increasing the fabrication cost [154,155]. Different with normal FDM printers that are operated at low temperature (≤280 °C), these specialized printers have better thermal management, higher heating capacity and stronger resistance to high temperature that these engineering thermoplastics need. Normally, FDM processing of these polymers aims to high value-added field like

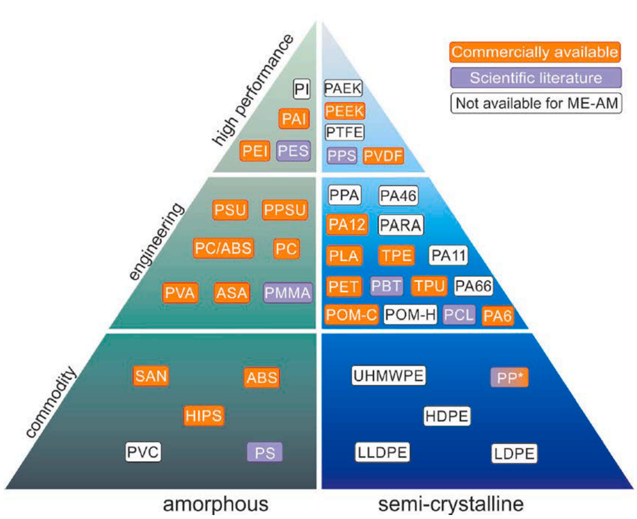

Fig. 13. Pyramid of polymeric materials as a function of the material availability in FDM market [152].

aerospace and biomechanical applications.

Most of these thermoplastics are amorphous as their low T_g and large viscous softening range can facilitate the extrusion and deposition of plastic beads. However, amorphous polymers normally have weak chemical resistance and low mechanical performance (e.g. Young's modulus between 1.9 and 2.4 GPa, and elongation at break between 3 and 9%). In contrast, the limited amount of semicrystalline thermoplastics have a drastic change in viscosity due to a very small temperature range for softening. Despite their difficulty in FDM processing, these polymers exhibit wider mechanical properties than amorphous counterparts (e.g. Young's modulus between 0.8 and 4 GPa, and elongation at break between 2.5 and 1600%) [152,156]. In order to make full use of respective advantages from each material, two or more polymers can be blended during the HME of filaments. One typical example is ULTEM® 9085 from Stratasys, a blend of PEI and PC. With the incorporation of PC, this commercial filament not only possesses lower Tg for easy extrusion, but presents better flowability, ductility, transparency, strength and stiffness [157]. Due to the high cost of Stratasys ULTEM® 9085 (~200 $/kg), Cicala et al. studied the fabrication of PC/PEI blends by varying the PC content and found that the standard PEI modified with 10 wt% PC outperformed ULTEM® 9085 in terms of thermal and tensile properties, which shows a great potential in the development of polymer blends for better performance [158].

4.2. Discontinuous fibers in FRPC

A wide variety of discontinuous fibers with varying sizes have been incorporated into the FDM fabrication of FRPC. According to their source, these fibril fillers can be classified into two categories: synthetic fibers and natural fibers. The former includes carbon fiber (CF), glass fiber (GF), Kevlar and liquid crystalline polymer (TLCP) and the latter has hemp, bamboo, flax, jute, harakeke and wood [159–162]. The synthetic fibers employed for FDM composites have numerous advantages such as lightweight, corrosion resistance, flame retardancy, chemical resistance and superior stiffness and strength while the natural fibers are normally biocompatible, biodegradable, renewable, recyclable and relatively cheap. Since the majority of natural fibers are unstable at temperature ≥ 200 °C, polymer matrices that require high processing temperatures in HME and FDM will be not suitable for the manufacturing of AM composites [163]. The mechanical properties for FDM-fabricated discontinuous FRPC has been listed in Table 1.

As the primary filler, the fiber content plays a crucial role in the overall properties of printed composite parts. By compounding and extrusion of CF/PA mixture via TSE and SSE processes, Liao et al. fabricated the composite filaments with varying fiber contents (0, 2, 4, 6, 8 and10 wt%) and comprehensively characterized the material properties after FDM printing. The high stiffness of CF promoted an upward trend in tensile and flexural performance with the increase of fiber contents while the impact strength presented a sharp loss at low CF contents. This can be attributed to the generation of stress concentrations at fiber ends, initiating the crack propagation. With the increase of CF loading, the crystallization behaviour of PA composites didn't have a big change since the existence of CF acted as not only an inhibitor in the motion and arrangement of molecular chains, but a beneficial nucleating agent to facilitate polymer nucleation. Results also showed the increasing thermal conductivities at higher CF contents due to the establishment of this fiber-induced conductive network. The positive correlation between tensile properties and fiber contents was also observed in the 3D printing of natural fiber (hemp and harakeke) reinforced PP composites by Stoof and Pickering. Nevertheless, the FDM composites had lower strength and modulus than those of feedstock filaments. The lower pressure in FDM process incurred stress relaxation and formed more voids as stress concentrators. Natural fibers also proved to be a remarkable filler to maintain dimensional stability with much less shrinkage [164]. The discontinuous fiber loading in FDM is normally less than around 50% composites because higher contents may

Table 1
List of mechanical properties for FDM-fabricated discontinuous FRPC.

Source	Polymer matrix	Fiber reinforcement	Fiber content (wt %/vol%)	Initial fiber length (mm)	HME	Tensile strength (Mpa)	Young's modulus (GPa)
[188]	ABS	CF	5	0.1	SSE	26.5	1.3 (+44%)
[189]	ABS	CF	10	0.1	SSE	37.4 (+32.6%)	0.79 (+58.0%)
[171]	ABS	CF	10, 20, 30, 40	3.2	Ram	~67.0	~14.5
[167]	ABS	CF	3, 5, 7.5, 10, 15	0.1, 0.15	/	42.0 (+23.5%)	2.5 (+31.2%)
[184]	ABS	CF	5	/	/	36.8	1.1
[190]	ABS	CF	15	/	/	39.05 (+41.0%)	5.9 (+141.3%)
[169]	PLA	CF	15	0.06	/	53.4 (~0%)	7.5 (+123.4%)
[175]	PLA	CF	15	/	/	38.2	/
[191]	PLA	CF	15	0.1	/	/	/
[166]	PLA	CF	3, 5, 7, 10	0.1	SSE	~55.0	/
[186]	PLA	CF	12.6	0.07	/	68.4 (+14.0%)	9.28 (+162.9%)
	ABS	CF	16.8	0.05		50.9 (+33.2%)	7.15 (+212.2%)
	PET	CF	17.7	0.07		68.3 (+48.2%)	8.47 (+313.2%)
	Amphora	CF	11	0.05		49.3 (+5.1%)	3.93 (+95.5%)
[192]	PEKK	CF	30, 40	/	/	/	/
	PPS	CF	40, 50				
[193]	PA12	CF	2, 4, 6, 8, 10	15–20	TSE + SSE	93.8 (+102.2%)	3.58 (+265.9%)
[194]	PA6	CF	/	/	/	~21.0	1.29
[172]	PA	CF	15	0.1	/	83.8	4.6
[185]	TPU	CF	0, 1, 2, 4	/	/	~24.0	~0.64 (+34.07%)
[178]	ABS	GF	15, 20, 25		TSE	58.6	/
[195]	PP	GF	30	/	/	~39.0	~1.4
[177]	PP	GF	30	/	/	~34.0	~0.4
[196]	PP	TLCP	20, 40	/	SSE	37.0	2.7
[164]	PP	Hemp fiber	10, 20, 30, 40, 50	≤ 8	TSE	22.45 (+31.9%)	2.00 (+181.0%)
		Harakeke fiber				23.55 (+38.4%)	2.09 (+193.7%)
[197]	ABS	Jute fiber	5	/	TSE	25.9	1.54
[176]	PLA + polyhydroxyalkanoate (PHA)	Wood fiber	15.2 ± 0.9	/	/	46.0	3.29

decrease the melt flowability and clog the nozzle [165]. In addition, some papers reported worse mechanical performance at high fiber loadings owing to the increase of porosity, which indicates the importance to eliminate this defect so that the benefits of fiber incorporation can be maximized [166,167].

Fiber length is an important factor in the limited improvement of strength for FDM-made discontinuous FRPC. Although initial lengths are long enough to promote the stress transfer from fiber to matrix,

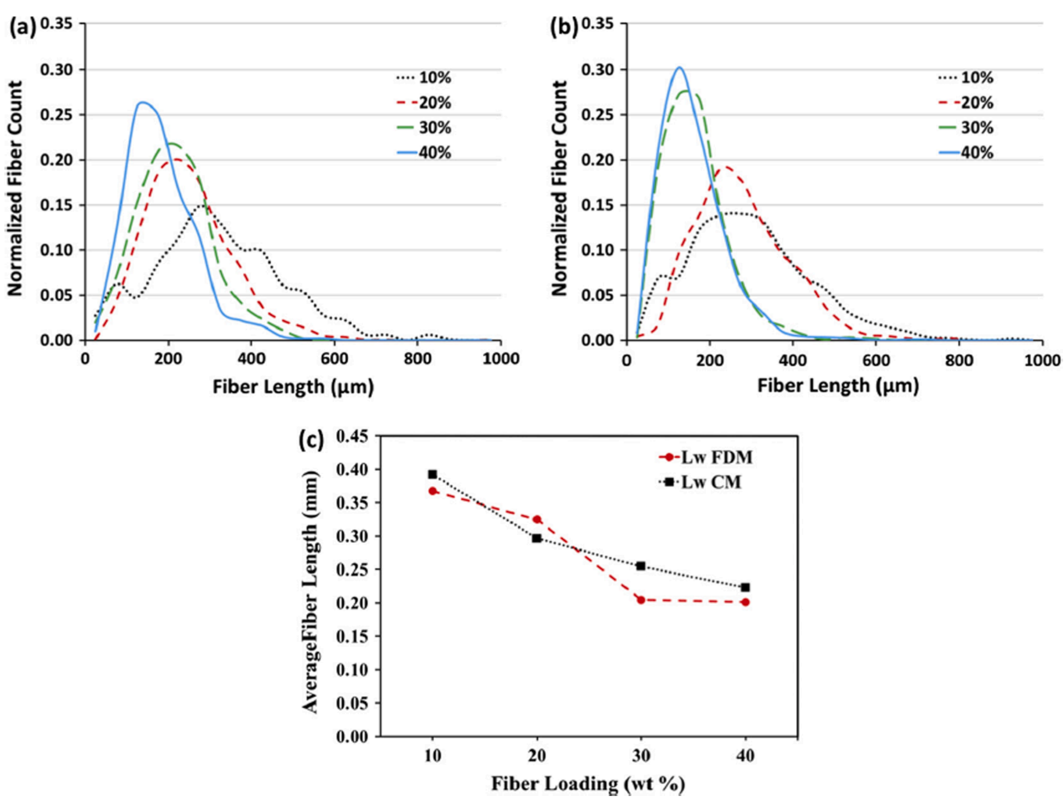

Fig. 14. Fiber length distributions as a function of varying fiber contents: (a) compression-molded, (b) FDM-printed, and (c) weight average fiber lengths of dog-bone samples [171].

discontinuous fibers are largely shortened by the high shear force in mixing and extrusion of rotating screws during the HME process, resulting in fiber lengths around one order of magnitude lower than the critical length [168]. Instead of fiber rupture under the external loading, these micro-scale fibers in composite filaments as FDM feedstock pull out of matrix without the effective transferring of the applied stress [169]. Moreover, shorter fibers can incur more stress concentrations with increasing fiber ends at the same fiber content [170]. Ning et al. printed ABS composites with the CF lengths of 150 μm and 100 μm and found that the longer fiber endowed the FDM composite with larger tensile strength and stiffness [167]. Tekinalp et al. analysed fiber length distributions both in FDM- and compression molding (CM)-fabricated samples. Results showed that compared to the initial length of 3.2 mm before the HME, the majority of fibers in FDM composites were broken down into the length of less than 0.4 mm. With the increase of CF content, fibers in FDM samples became shorter since more fibers were damaged due to the increasing interaction between these fillers. In contrast, composites made from CM had slightly longer fibers, crediting to the lower shear applied onto the material (Fig. 14) [171]. Blok et al. also investigated the composite printing by respectively using short fiber (~100 μm) and continuous fiber feedstocks. Although much higher mechanical performance was observed in continuous FRPC, design freedom was largely compromised with the incapability of free deposition through small steering radii and sharp angles. Filaments with short fibers exhibited better printability and higher degree of design freedom [172]. Undoubtedly, there is a great promise in the production of high performance complex FRPC if the printed fiber length can be increased in this HME + FDM system.

During the extrusion process, a high shear force is generated between the semi-liquid composite flow and the inner wall of nozzle, contributing to the fiber alignment along the printing direction. To be specific, the external force from the feed roller pushes the composite melt into the nozzle with a small diameter, leading to a high velocity gradient and thus great shear stress in the flow direction. Fibers are forced to be aligned along the axis of nozzle so as to reduce the flow resistance. These highly oriented fibers are preserved after depositing onto the build plate due to the fast cooling and solidification [173,174]. Higher fiber loadings contribute to more uniform fiber alignment. As a result, the anisotropic feature in FDM-based parts is further aggravated with the incorporation of fibers, whether in structural distribution or in mechanical properties. The tensile strength in the build direction normally is only 50–75% of in-plane strength while the fibril fillers increase the anisotropy with the reduction of out-of-plane strength close to 90% [175]. Inspired by the traditional z-pinning concept to improve through-thickness performance and avoid delamination, Duty et al. introduced this scheme into the FDM process, where the part was conventionally printed with staggering seams designed to be z-axis aligned throughout the structure. This length and position of these seams can be controlled and filled by extruded pins prior to the deposition of subsequent layers (Fig. 15). Results showed that the z-direction strength and toughness of

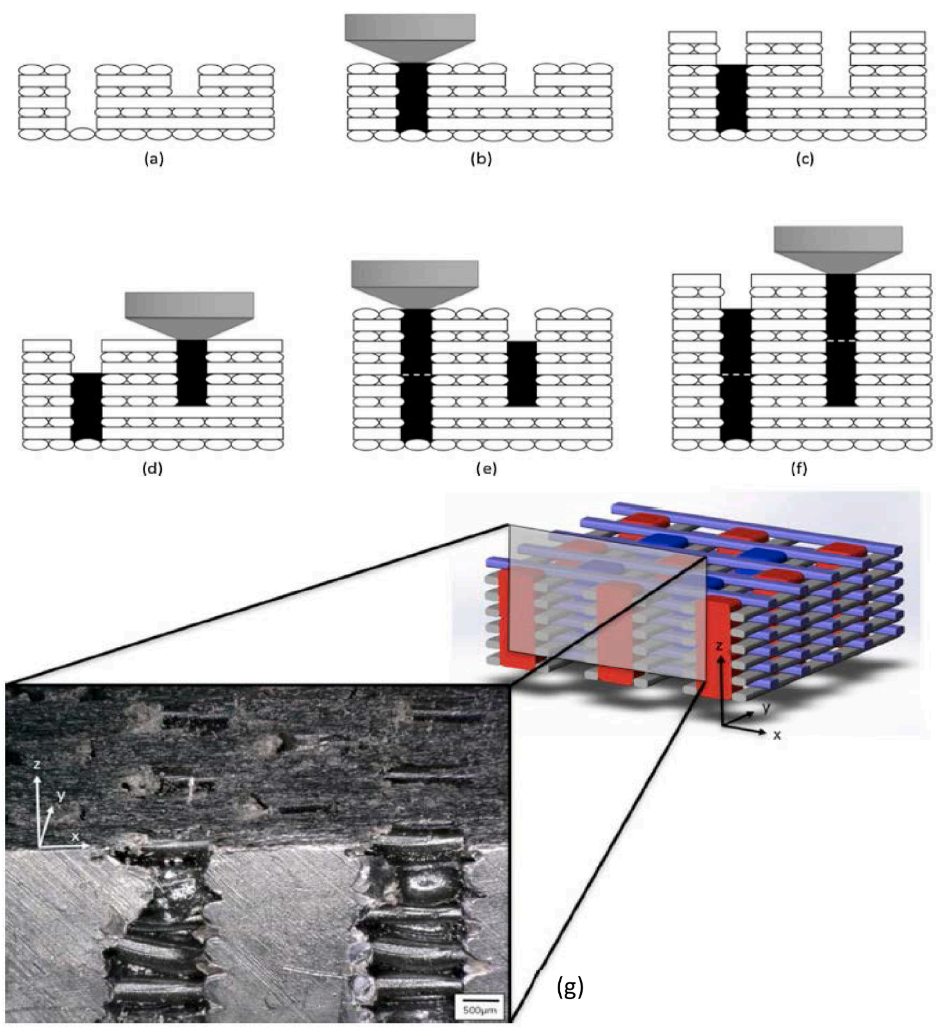

Fig. 15. Z-pinning approach for FDM printing mechanically isotropic materials: (a-f) process steps for 3D printing with z-pinning; (g) cross section of printed sample with 120% pins [175].

printed CF/PLA composites can be enhanced by more than a factor 3.5, and even higher than x-direction strength after normalizing these values. The printed part with the largest pin volume also demonstrated isotropic properties in mechanical characterization [175]. This strategy builds a new platform for AM designers to customize directional properties that are independent of print orientation.

The formation of voids has been discussed above as the consequence of insufficient bonding between adjacent beads in FDM process, yielding a detrimental impact on the mechanical properties and structural integrity for the printed parts. Thus, discerning the change of pores and voids after the introduction of discontinuous fibers is essential to ensure the printing quality of FRPC parts. Tekinalp et al. investigated the microstructure of FDM-based CF/ABS composites and found that in addition to the triangular voids on the bead surface, internal voids inside the extruded beads started to form in the printed composites. The size of those relatively large triangular voids became smaller with the addition of fibers, which can be ascribed to the high thermal conductivity of CFs and the decreased die swell at the nozzle, contributing to the improved packing after bead deposition (Fig. 16). As a comparison, the authors also fabricated composite samples with the same feedstock materials via CM method and no visible porosity was observed due to its high pressure operational process [171]. Ning et al. illustrated the same void changes and varieties with the incorporation of CFs into the ABS matrix. Meanwhile, the porosities at different fiber contents were calculated, showing a V shape trend from 0 to 15 wt% CF contents with the lowest value at the 3 wt% fiber loading [167]. Due to the increased stress concentrations from these voids, it to a certain extent explains why a higher CF content didn't impart a better mechanical performance of FDM composites in this paper. The defect of inner-bead voids is mainly caused by the weak interfacial adhesion between fibers and polymer matrix. Fig. 17 depicts the inner-bead and inter-bead voids inside the FDM printed fiber reinforced composites. However, higher porosity can facilitate more swelling in printed biocomposites (e.g. wood fiber + PLA matrix), shifting this drawback into an advantage in designing programmable moisture-actuated hygromorph products [176]. Although various plasticizers and compatibilizers have been added to the FDM composite matrices with improved mechanical properties (e.g. flexibility and handleability), few is related to the surface modification of fibers for better interfacial bonding [177–179]. Since most of these fillers are synthetic fibers with no active groups and smooth surface, it's difficult to form a strong fiber–matrix adhesion by merely using the unmodified fibers as the reinforcement. Some reviews have focused on the enhancement of this interphase in conventionally manufactured composites via various surface treatment approaches (e.g. sizing, coating, grafting, etc.) [180–183]. This enlightening information may inspire material researchers, scholars and experts to develop AM-based FRPC with superior fiber–matrix interfacial properties so as to achieve better mechanical, thermal and electrical performance.

Apart from the material properties, it is vital to understand the influence of various processing parameters in FDM on the morphology and overall performance of FRPC, including deposition parameters (e.g. infill pattern, infill density, layer thickness, bead width, build orientation, etc), operation parameters (e.g. nozzle temperature, nozzle size and shape, feed rate, print bed temperature, etc.) and ambient parameters (e.g. humidity, temperature, etc.). Based on the own-made 5 wt% CF/ABS composite filament, Ning et al. investigated the tensile properties as a function of raster angle, infill speed, nozzle temperature and layer thickness. Using X axis as the benchmark during printing, raster angle of [0, 90] presented much large tensile strength, yield strength and Young's modules than those from raster angle of [+45, −45], which can be attributed to effective load transfer from the matrix to reinforced CFs. This was also proved from the facture interface after tensile test that

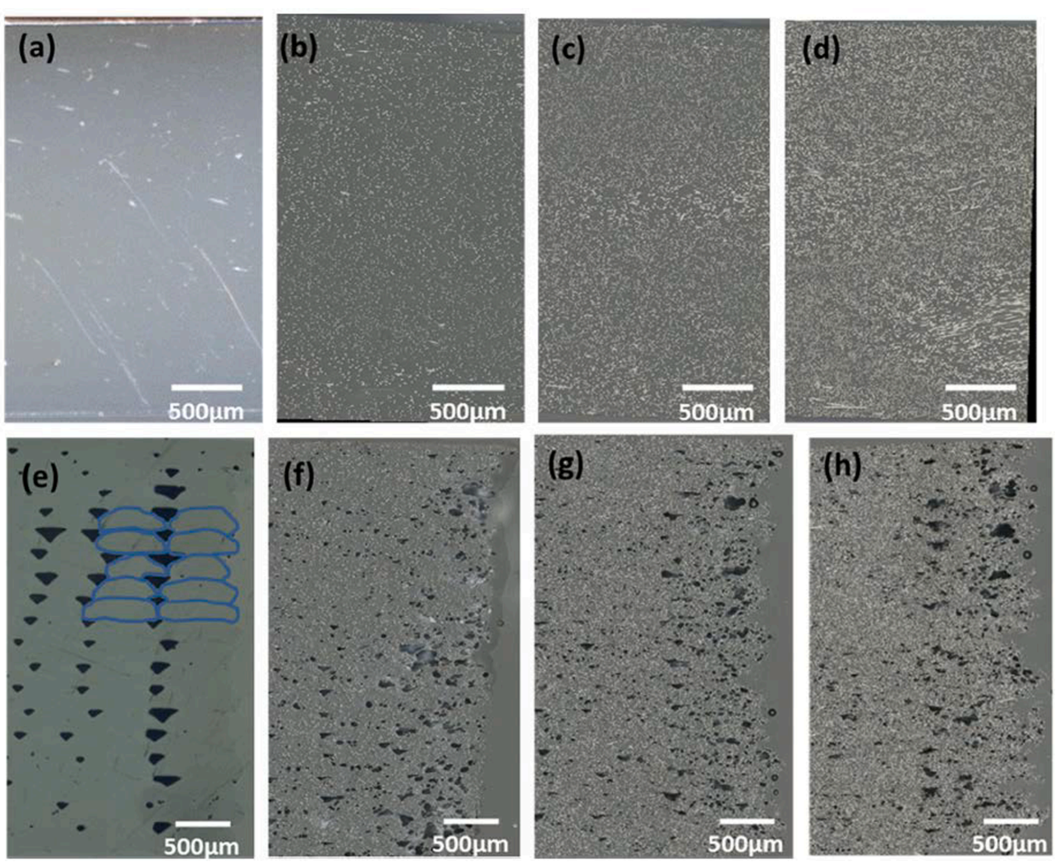

Fig. 16. Micrographs of polished surfaces of CF/ABS samples fabricated by CM and FDM methods: (a) CM neat-ABS, (b) CM10%CF, (c) CM20%CF, (d) CM30%CF, (e) FDM neat-ABS, (f) FDM10%CF, (g) FDM20%CF, and (h) FDM30%CF [171].

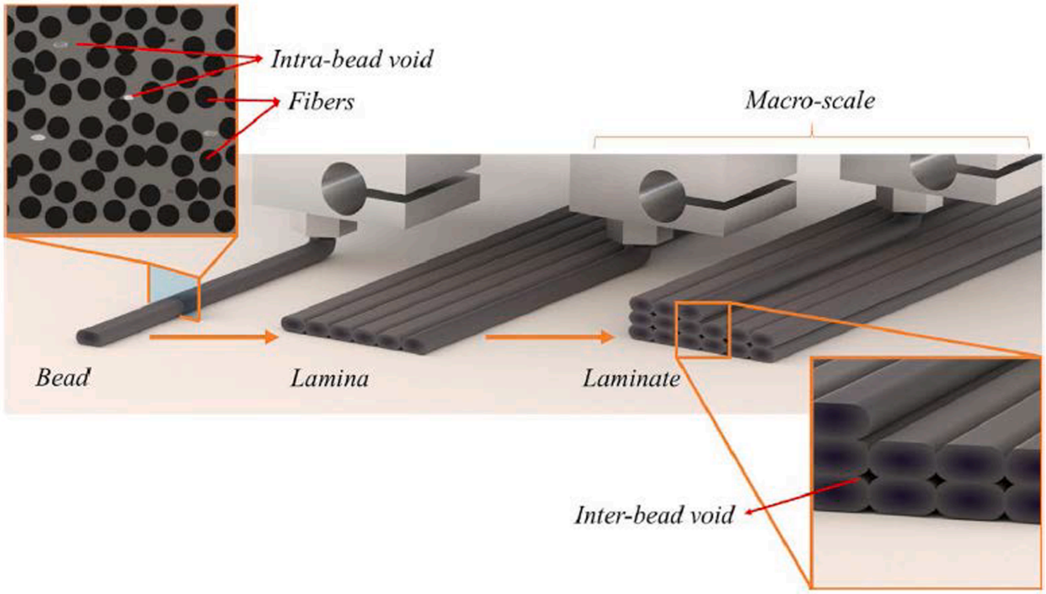

Fig. 17. The schematic of the multiscale structure of FDM-fabricated fiber reinforced composite parts with inner-bead (intra-bead) and inter-bead voids inside [84].

fibers were ruptured for [0, 90] samples rather than pulled out for [+45, −45] counterparts. The best infill speed was found at 25 mm/s since faster speed caused less interaction and poorer intra-/inter-layer bonding between deposited beads. With the altering of nozzle temperature, a peak point for tensile performance appeared at 220 °C since beads cannot firmly bonded together at lower temperature while porosity in printed composites increased at higher temperature owing to the polymer degradation. Although 0.25 mm layer thickness contributed to the higher toughness and ductility, tensile strength and stiffness exhibited the best values at the layer thickness of 0.15 mm by virtue of the tighter coalescence between each layer [184]. Shifting bead layout orientations from 45° to 0°, Anwer and Haguib reported higher mechanical performance for TPU composites with varying CF contents from 0 to 4 vol%, suggesting larger stiffness imparted by the fiber at the 0° print. To further elucidate the fiber orientation, they observed higher water contact angle from the 0° printed composite than that from the 45° bead orientation via hydrophobicity test, indicating greater entrapment from the higher fiber alignment at the smaller angle [185]. Jiang and Smith also studied the correlation between tensile properties and bead orientations at four angles (0°, 45°, ±45°, 90°) relative to the load direction. Compared to the pure polymers, results showed that CF reinforced composites in general had higher tensile modulus at all print orientation while less improvement and even a decrease were observed for tensile strength except at the 0° print orientation [186]. This could be the low conformity of CFs to the previous layer, thus reducing the contact area for neighbouring layers during printing. This phenomenon has been reflected on the work from Love et al. that the out-of-plane tensile properties of the pure ABS was better than that of CF reinforced composites [187].

4.3. Support materials

The incorporation of support into designed parts is necessary for the printing of complex geometries when overhangs and cavities are suspended in the mid-air. The increased fabrication freedom also enables designs with freely moving parts inside once the support is removed. Currently, there are three types of support materials employed in FDM: build materials, breakaway materials and soluble materials. The first type is mainly used for single-nozzle printers where the support material is the same with the thermoplastic filament for the model building while a low-density format is usually chosen for the support so that it can be broken off after printing. Although material compatibility is remarkable in this economic approach, more effort is required for support removal and yield poor surface quality, to a certain extent compromising the structural accuracy. The second type is like the first one while a separate polymer material is deposited with the build material. It's quicker and easier to be peeled off and leave a clean surface without the need of post-processing. Nonetheless, the compatibility of breakaway materials due to their less adhesion is still a concern, especially for multi-material 3D printing [22]. Instead of requiring manual removal, the last type can be dissolved away in the proper solution. They allow for the fabrication of dense and intricate geometries where normal tools cannot reach into the support. Two soluble polymers are widely utilized in this type: polyvinyl alcohol (PVA) and high impact polystyrene (HIPS). The first one is a hygroscopic, biocompatible and flexible thermoplastic that can be directly dissolved into water while the second one has lightweight, rigid and impact resistant properties that needs to use proper chemical solvents like limonene [198,199]. The main drawback for soluble materials as the support is the long dissolving time. To enhance their removal efficiency in printed parts, some processing strategies have been attempted to improve solvent dissolution, such as the increase of temperature, the application of agitation and/or the introduction of other solvents (e.g. hydrogen peroxide) [200–202]. Up to now, there is no relevant report on the effect of varying support materials on the interlayer bonding with FRPC-based build materials, which is imperative to fulfil the FDM printing of complex composite objects with precisely designed dimensions.

5. Large-scale FDM

Since most of the commercialized FDM systems only offer a small-scale fabrication capacity with small building volumes of 0.03–0.3 m^3 and low printing speeds of 15–85 cm^3/h, it greatly restricts the feasibility of these 3D printers in the industrial manufacturing of large parts and tooling on the order of several to dozens of meters [203]. A special research has been focused on the goal to achieve the fastest deposition rates, the maximum printing size and the highest material throughput. In collaboration with Lockheed Martin, Oak Ridge National Laboratory (ORNL) developed the first Big Area Additive Manufacturing (BAAM) system with the moving speed of the deposition head reaching at 12.7 cm/s in the X-Y plan [204]. Later, ORNL improved this large-scale AM system with Cincinnati Incorporated©, featuring the build geometry of

6 m × 2.5 m × 1.8 m and the maximum material output up to 45 kg/h [205]. This new system possesses the capability to print 10x larger parts at 200x faster speed with 20x cheaper prices compared to desktop FDM systems. Meanwhile, a Large Scale Additive Manufacturing (LSAM) system created by another company named Thermwood Corporation© exhibited an even higher material output rates at 227 kg/h with the maximum building size of 30 m × 3 m × 1.5 m [116]. Relative to the 3D printing of large components using regular temperature polymers like ABS, Purdue University invented the Composite Additive Manufacturing Research Instrument (CAMRI), a medium size extrusion deposition printer that can not only print high temperature polymers (e.g. PPS) with the reinforcement of high CF contents (50 wt%), but provide a valid simulation tool to predict the outcomes of a designed print structure that arises from the extrusion deposition based AM process [206,207].

Distinct from the operation principle of FFF technique, large-scale AM systems (i.e. BAAM and LSAM) are capable of directly utilizing pellets as 3D printing feedstocks rather than filaments due to the organic integration of HME process into the deposition head. The extra procedure of converting pellets into filaments before AM is therefore eliminated with the feedstock cost decreased from $50–100/kg to under $10/kg [208]. For a BAAM machine based on this extrusion deposition AM method, a customized SSE with high extrusion rates is attached to a 3-axis gantry system, through which thermoplastic pellets are fed, melted and conveyed into the printing nozzle so that they can be deposited onto a large heated substrate (Fig. 18). In contrast to the small diameter of nozzles (less than 1 mm) in conventional FDM printers, the nozzle sizes of large-scale AM machines normally range from 5 to 10 mm dependent on the requirement of printing resolution and speed [209]. By using a printed mold from BAAM as an example, Post et al. discussed the economic efficiency of this technology and found that 17× reduction in manufacturing cost and 50x reduction in manufacturing time can be realized for the composite tooling industry [210].

Owing to the high CTE of thermoplastic polymers and big temperature gradients existing in neighbouring layers, residual stresses are commonly accumulated in BAAM from the non-uniform shrinkage when the previous layer has already cooled down and thermally contacted before the succeeding deposition of a hot layer. The huge residual stress in BAAM's large part deteriorates the 3D printed formation of accurate geometry, leading to the occurrence of warping and delamination, and even the failure of AM fabrication [211]. The inclusion of CF has become a rule of thumb to avoid these issues for its near-zero thermal expansion along the fiber axis [212]. Apart from the increased thermal conductivity and enhanced dimensional integrity, the high stiffness and strength of CF also result in a positive impact in improving the mechanical performance of BAAM thermoplastic materials [187,213]. Nonetheless, the incorporation of discontinuous CF confines the decrease of thermal gradients and part distortion to the printing direction while the CTE in the transverse direction is still governed by the polymer matrix, which can be attributed to the induced alignment of CF along the movement of deposited beads based on the convergence zone in nozzles and shear alignment effects [113]. The strength transverse to the printing direction is thus less than that parallel to the bead deposition. In order to improve transverse properties and maintain the dimensional fidelity of in-plane geometry, mechanical compaction was recently adopted in the modification of CAMRI with a tamper system attached onto the printing nozzle to squeeze the flow of molten materials and fill the voids between extruded beads [214].

To date, the application of 3D printed parts as load-bearing elements via large-scale AM techniques is still limited partly because of the mechanical anisotropy. Instead, various tools and molds have been printed for the conventional polymer composite manufacturing, such as VARTM and hand layup molds for low temperature fabrication, as well as autoclave and compression molding tools for high temperature applications [205,215–217]. These large-scale printed composite tools not only necessitate lower cost and shorter lead time, but present better dimensional stability with negligible deviations after even ten cycles of manufacturing process [205]. In view of the induced alignment of CF in the flow direction with corresponding low CTE compared to the transverse bead, the entire expansion of tools and molds can also be tailored by elaborately controlling the printing patterns so that a similar thermal properties with the molded material can be obtained for the production of high-quality parts.

Similar with the mechanical phenomenon in small-scale AM process, the existence of interlayer gaps also weakens the tensile strength of successive layers, resulting in the much lower mechanical performance in the z-direction. Via the addition of 20 wt% CF into ABS matrix, Duty et al. discovered that the out-of-plane strength of BAAM-fabricated composites (1.5 ksi) lost almost 85% compared to that from the in-plane test (9.5 ksi). They ascribed this poor interlayer strength to the reduced contact area and weak bonding between adjacent beads due to

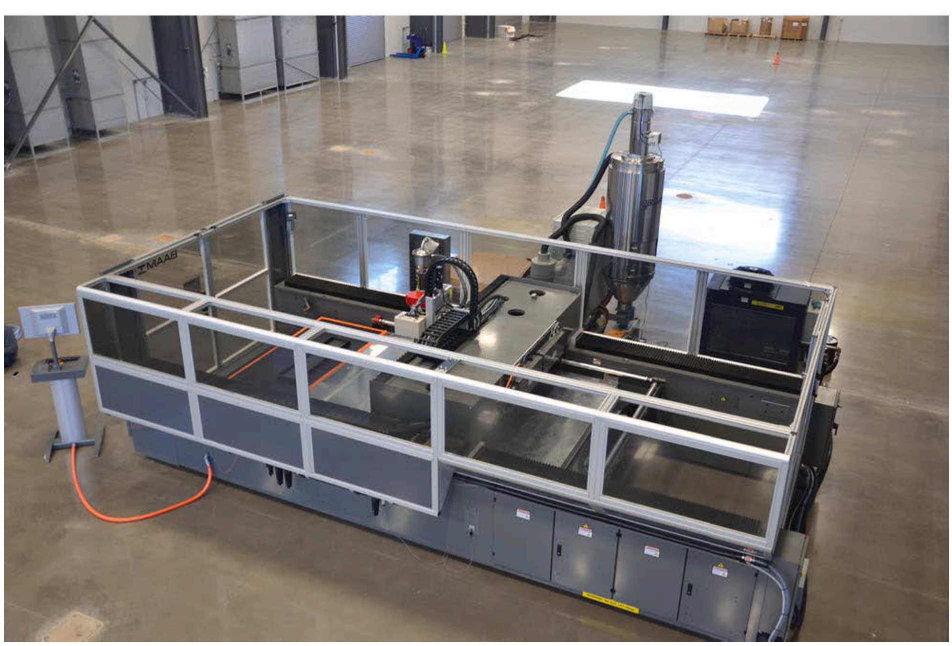

Fig. 18. BAAM system developed by ORNL and Cincinnati Incorporated [208].

their increased rigidity from the high CF content [218]. As the deposition of one layer in BAAM large articles takes a long time and the surface temperature of prior layer has already dropped below the T_g of the polymer material with the following layer printing, another factor regarding the impeding of intermolecular diffusion between the layers should also be considered since it could also lead to the poor interlayer adhesion [124]. Hence, increasing the surface temperature of the deposited layer will be an effective measure to enhance the interlayer bonding of the material. With the installation of infrared lamps into a BAAM system, Kishore and his team increased the substrate layer temperature to above T_g via this preheating technique before the printing of the next layer and achieved better interlaminar strength with doubled fracture energy under certain circumstances [219].

According to the special features of large-scale AM (e.g. larger printing size, thicker extruded beads and faster deposition rates), the possible delamination and warping of printed parts remain tricky issues although the introduction of CF can reduce internal stresses. Even a small thermal strain may give rise to several millimeters of deformation considering these magnified defects at large sizes [220]. For instance, in partnership with Local Motor, ORNL produced the world's first printed car via the BAAM system while the first trial was not very satisfactory with the accumulation of large thermal mass and the severe warpage and delamination between deposited layers [221]. Consequently, in-depth research of thermal evolutions in large-size composite fabrication based on varying material combinations and processing parameters is extremely essential to achieve desirable properties under this high-throughput AM process. By capitalizing on a series of thermal characterization approaches (e.g. DSC and TGA), Ajinjeru et al. analysed the glass transition temperatures and degradation profiles of PEI and 10 wt % CF/PEI pellets to identify the upper and lower thresholds for appropriate processing temperature ranges with the view of imparting excellent strength and modulus to the end part. They found that the increase of processing temperature had a strong impact on the viscosity of PEI with the decrease up to 50% while the addition of CF into this thermoplastic matrix yielded a 108% increase for its viscosity, which indicates the importance to build a close correlation between processing parameters and the rheological behaviour of candidate materials for BAAM fabrication [222]. Compton et al. developed a simple 1D thermal finite difference model to predict layer temperatures of BAAM-made thin wall sections using CF/ABS composite materials and compared these results with corresponding experimental measurements through infrared imaging (Fig. 19). A high-level matching was observed with the indication that the steady temperature of the top layer and ambient temperature in the build chamber are crucial to minimize the likelihood of deformation for printed large objects. However, higher thermal conductivity from the incorporation of CF showed a detrimental effect on the printing size of this structure since more heat was lost with the increase of wall surface area [220]. Conspicuously, a further exploration of temporally and spatially complex thermal evolutions combined with printing conditions, geometry and material properties will be helpful in the understanding of internal stress accumulation, deformation and bead fusion in the large-scale AM process.

Currently, the fabrication of short CF reinforced composites via large-scale AM methods (i.e. BAAM, LSAM and CAMRI) is mainly dependent on the empirical calibration with tedious trials and errors required to systematically optimize the manufacturing process. It's time-consuming, energy/materials-wasting and only limited to a certain printing scale. Hence, the development of process simulation tools to

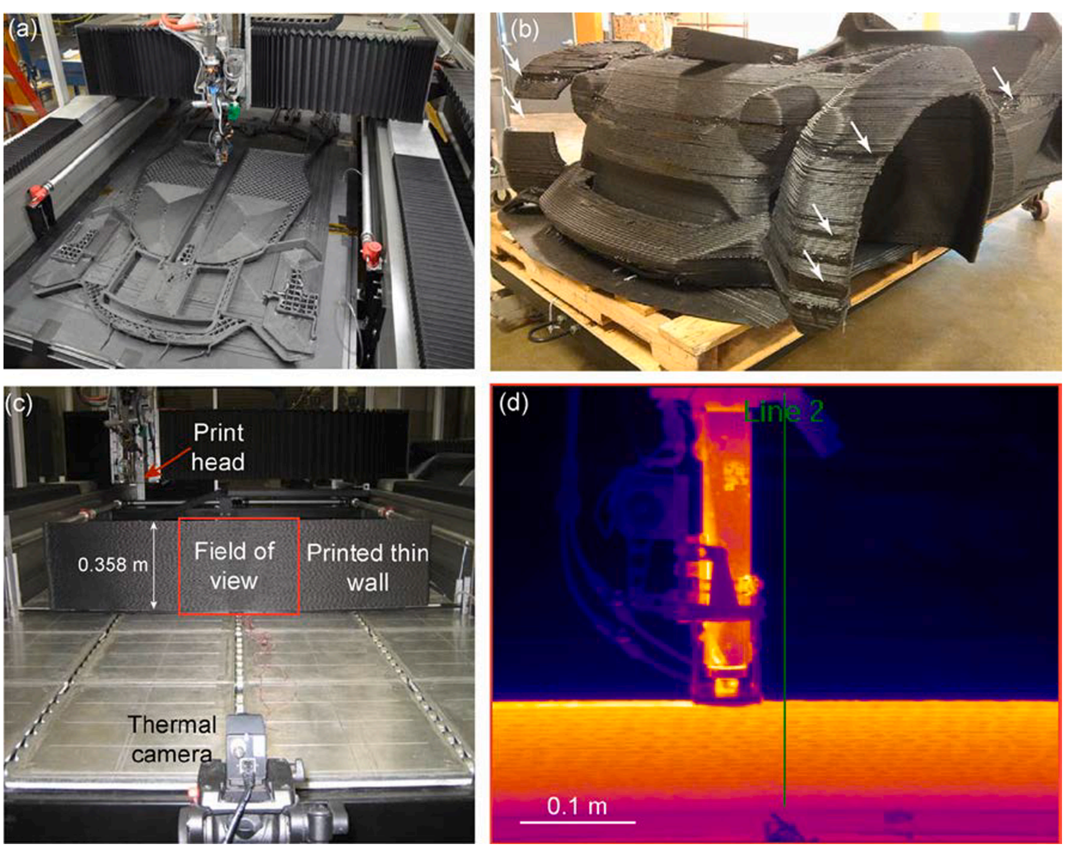

Fig. 19. Thermal analysis of CF/ABS composites fabricated by large-scale FDM system: (a) photograph of a full-size car chassis being printed on the BAAM-CI system; (b) photograph of the printed car chassis, in which several cracks, labelled with white arrows, have initiated from the thin fender sections due to the high cooling rates in these thin regions; (c) experimental setup showing the thermal camera, the approximate size of the view frame, and a printed thin wall on the BAAM-CI print bed; (d) a representative thermal image of the thin wall during the printing process, in which orange and yellow represent higher temperatures and blue and black represent cooler temperatures [220]. (For interpretation of the references to colour in this figure legend, the reader is referred to the web version of this article.)

predict specific outcomes of designed parts from the modelling of various manufacturing profiles is preferred in this field research. By integrating multi-scale damage mechanics and linear elastic fracture mechanics into finite element method [223–227], Talagani et al. created a computational tool with a fully coupled thermo-mechanical analysis ability to the extrusion deposition based AM of polymer composites, in which problem areas prone to high residual stresses and crack formations can be identified in this simulation model [228]. Taking material properties into account, Brenken and his co-workers developed a physics-based simulation tool Additive 3D in Abaqus© 2017 to theoretically investigate the AM process of fiber-reinforced thermoplastic composites in CAMBRI printer. Without the need of additional calibrations, physical properties of 50 wt% CF/PPS composites (e.g. crystallization kinetics, thermoviscoelastic stress relaxation and material shrinkage behavior) were first characterized via corresponding experiments and then modelled using this customized tool, demonstrating an accurate prediction (less than 7% relative deviations) for residual stresses and final deformations of printed structures [229]. Advanced simulation tools incorporating comprehensive material portfolio, extrusion deposition-based process mechanism and product performance analysis are still in demand in light of the sensitivity of different large-scale AM configurations to product quality and significant consumption of materials and time during each printing.

6. Multi-axis FDM

Although the recent development of large-scale FDM ushers in the industrial revolution for the manufacturing of large thermoplastic composites (with all current applications focusing on discontinuous high-performance fibers as the reinforcement), the inherent operational mechanism of these commercially available FDM printers is still built upon the gantry-style CNC machine with three-axis Cartesian coordinate system to move the extruder head [230]. As the incapability to rotate the extruder head during printing, its motion is restricted to only translate in the horizontal x-y plane while the vertical z movement is executed intermittently after each layer deposition. This 2D layer pattern in FDM-fabricated parts has a negative influence on the mutual bonding between neighbouring layers, forming weak boundaries with significantly less strength and ductility [231]. The inconsistent material properties underlying this anisotropic geometry impair the global mechanical performance of the printed object. Meanwhile, the conventional FDM technique is also problematic for the fabrication of cellular structures, especially for metamaterials with intricate topological designs [232,233]. These materials recently are booming in various fields for their exotic properties like negative poisson's ratios, negative bulk modulus and density, and negative refractive indices in electromagnetic waves, all of which are artificially manipulated by the internal geometries featuring small, complex repeating unit cells with hierarchical coverage from macro- to micro-scale arrangements [234–236]. It makes extremely difficult for this layer-based method to print lattice objects with numerous overhang structures since a vast amount of support materials are required, leading to the increase of fabrication costs and the reduction of production efficiency, let alone those with closed hollow cells in which the deposited supports are even impossible to be removed after printing [237]. Moreover, the right fiber orientation in composite fabrication is crucial to achieve the proper functioning of end parts. The FDM based process can only orient fibers in the plane of each deposited layer without the capacity to position them along out-of-plane directions. Therefore, the free distribution of fibers in 3D space based on this primitive planar layer deposition technique is insurmountable, resulting in the limited application for the attenuated performance of printed composites [238]. In order to overcome these barriers caused by the single-plane layering process, the concept of multi-axis AM possessed with higher degree of freedom (DoF) is undergoing intense development based on its tremendous potentials in multi-plane printing [239]. Besides, the introduction of additional DoF can not only shorten the build time with less setup alterations, but minimize the stair-step effect and improve the surface quality of printed parts by reducing relocation and re-positioning in the deposition process [240,241]. Since the multi-axis FDM is still an emergent area with scarce research, to authors' best knowledge, there is no specific work at present on the fabrication of discontinuous fiber reinforced composites via this approach but relevant studies for this field will be discussed hereinafter that could be extended to explore the application of multi-axis 3D printing into fiber/polymer composite system.

The simplest strategy to realize the multi-plane printing is to integrate a rotatable building platform with the commercial 3-DoF printers. By modifying a standard low-cost FDM printer with a rotatory cuboidal platform, Gao et al. presented a "RevoMaker" system in which an extra 1-DoF was added to the cuboid so that the multidirectional rapid prototyping process can be conducted through depositing PLA polymer onto the different cuboidal base facets, simultaneously reducing the time and support material consumptions [242]. However, for intricate structures with long, slender protruding and massive curvy lines, support generation or sub-cuboids for further partitioning of 3D parts are still needed using this approach. Differing from slice-wise 2D motions in conventional FDM method, Wu and his team included two extra DoF into a standard delta 3D printer with two rotation axes for the building platform, enabling arbitrary 3D movements for lattice mesh printing. A collision avoidance algorithm was also created for this 5-DoF wireframe printer while the computation efficiency remains a big issue for dense meshes [243]. To facilitate multi-plane motions between an accumulative tool and an object, Song et al. developed a 6-axis FDM system by employing six relatively cheap linear actuators to move the printing head and an embedded laser camera to correct backlash errors for higher deposition accuracy. Apart from depositing the thermoplastic material (i.e. ABS) in multiple directions, this system opened the door for more toolpath planning like non-planar layering in the AM process [244]. Other related configurations based on parallel mechanism have also been proposed to manipulate the structural DoF via regulating the corresponding rotation and translation motions, which may give useful ideas for engineers to achieve more flexible mobility in 3D printing platform [245–247]. Despite the merits of above multi-axis FDM schemes and their capacities to do multi-plane printing without the need of support structures for overhangs, the difficulty in further improvements of deposition rates, printable complexity and build scale is the biggest obstacle to fulfil the industrialization of these novel technologies.

As an automatically controlled equipment, industrial robotic arms have been widely utilized in a wide variety of assembly lines, excel at performing repetitive and precise tasks such as welding, cutting, polishing, painting, pick and place, product testing, inspection and so forth [248,249]. Compared to these cyclic operations with singular movements, robotic arms are being repurposed to the customized fabrication of complex and multi-functional materials with the advance of digital manufacturing technology [250]. According to the marketing survey and feasibility study conducted by Zhang et al., the interviewed service providers gave as high as 70% probability of using industrial robots in their AM processes [251]. In consequence, a new concept of combining FDM technique with multi-axis robot-manipulated system is becoming the hotspot in the latest years. Based on the adjustable freedom of motion via regulating the number and types of joints, the increased DoF of robotic arms can be exerted either on the build substrate or on the extrusion head of a 3D printing system [252–255]. For example, Wu et al. proposed a RoboFDM device by offering 6-DoF motions to the printing platform via the robotic arm so that molten filaments of PLA can be deposited along different directions from a fixed nozzle at the working frame. A decomposition algorithm was computed to sequentially print each segment of a model in a support- and collision-free fashion [256]. Instead of using the flat build bed, Brooks et al. fixed a fiberglass made concave platform onto the ABB robot's end effector so that thin shells with varying mesh shapes were printed onto this flexibly moving mandrel surface from a fixed extrusion head [254]. By installing a FDM extrusion system onto a 6-DoF robotic arm, Ishak demonstrated the multi-plane layering capacity of this robot AM printer to fabricate 3D lattice parts with no support structures. The flexible printing toolpath can be designed via the corresponding algorithm to obtain the desired mechanical properties [257]. Similar with the feeding mechanism in large-scale AM processes, McGee et al. added the thermoplastic elastomer (TPU) into a screw-driven extruder that was mounted to a 7-axis robot and deposited this melted material onto a heated aluminium bed to form a monolithic elastic net with tailored anticlastic features. This system was created for the fabrication of lightweight spatial enclosures with dynamic reconfigurations and minimal material usage [258]. Tam and Mueller integrated a custom-designed heater with the 6-axis KUKA small robot to explore a new approach of material printing called Stress Line Additive Manufacturing. Structural behaviours of printed objects in terms of geometry, topology and bead layout were experimentally characterized, exhibiting better mechanical performance than the conventional layer-based paradigm [231]. Most other relevant cases regarding the employment of multi-axis robotic arms in FDM process also focus on the extrusion head as the end effector, which may attribute to the easier toolpath planning, higher deposition accuracy, larger moving flexibility and more complex printability for this modification type.

With the assistance of various industrial robots, the multi-axis FDM technology has gained popularity among architects, designers and engineers to fabricate construction elements at an architectural scale with their superior topological intricacy compared to those made by 3-axis layer-based large-scale AM counterparts. For the purpose of printing curved thermoplastic strips to form shell-like building part, Felbrich et al. equipped an industrial 6-DoF robotic arm with a customized flat slit-like printing head and six pneumatic cooling nozzles around its tip to facilitate the rapid crystallization of extruded material (Fig. 20). HDPE granulates were fed through an Archimedes' screw and printed out at an extrusion velocity of 0.8 mm/s to form each single strip with a width of 80 mm and a thickness of 2 mm. After printing a large-size closed shell, a strong loadbearing object was obtained via spraying concrete on the surface, showing the great promise of continuous free-form accumulating process [259]. Through mounting an ABB robot on a mobile platform, Hack and Lauer patented a method with the industry partner Sika Technology AG to robotically produce a series of 3D mesh architectural formworks with high capacity of precise spatial coordination (Fig. 21). Thanks to the movable robotic system, the FDM printed mesh mould can be varying sizes and cast with cementitious materials to meet different construction requirements [260,261]. Learning from the spider webbing behaviour (e.g. spining and weaving), Yuan et al. customized a printing tool consisting of one fixed nozzle and three flexible nozzles that can move synchronously around the central one in a regular manner (Fig. 22). Carried by a Kuka 6-axis robot arm, a rosary-like building structure with variable cross-sections was printed through the collaboration of collective nozzle depositions and programmable robot motions [262]. With the strategic alliance between robotic technology and FDM printing, it opens a new pathway to manufacture sophisticated architectural elements with a high degree of spatial and geometrical complexity. Nevertheless, the production rate of this robot-assisted AM technique still needs to be improved for the construction industry and the suggested solutions here can be the synergistic operation of multiple robotic arms and/or the development of faster multi-nozzle printing heads.

With the aim of further advancing the performance of 3D printed products to reach the standard for some specific applications, a wide variety of SM methods have been intelligently integrated with AM processes to create a hybrid manufacturing system. The advantageous combinations of multiple AM + SM approaches can not only circumvent individual technological limitations to fabricate parts with higher quality, but lower the threshold for some economical products with less lead time and higher material utilization efficiency [263,264]. In a hybrid manufacturing process, all these machines are usually coalesced into the same workspace and each of them can be utilized concurrently or independent of others' operations [265]. Up to now, most of additive-subtractive hybrid processes with multi-axis motions are heavily relied on the CNC machines to increase the DoF via rotatable building platform and thus the movements of AM or SM heads are still confined to

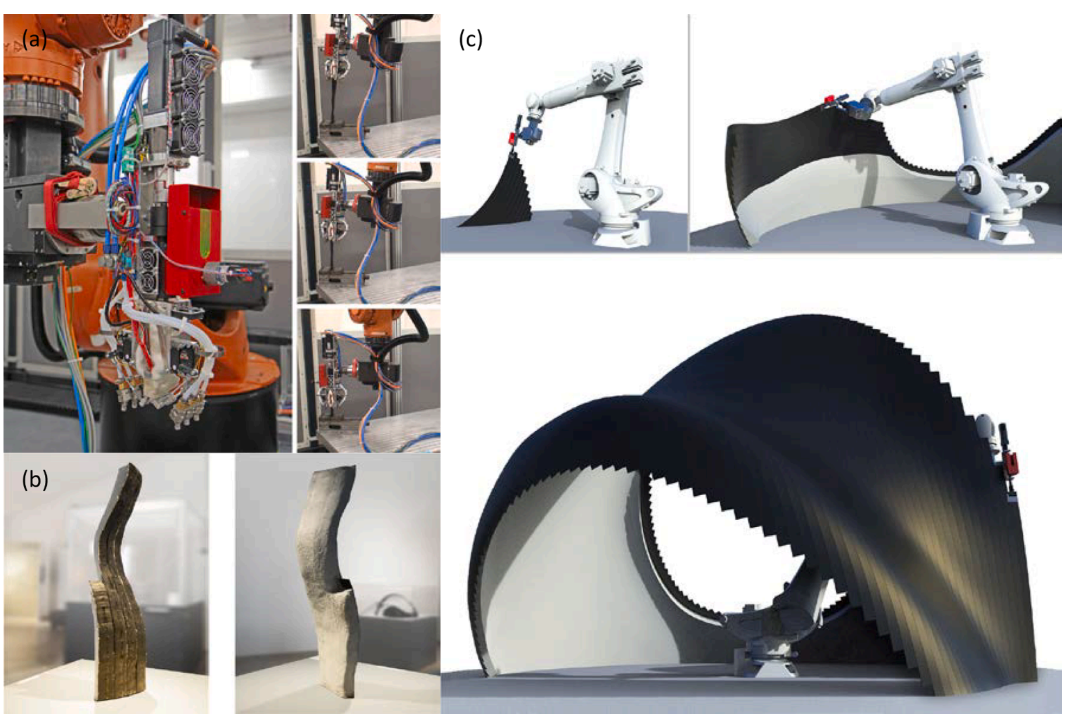

Fig. 20. The robot-based FDM system for composite shell construction: (a) the industrial 6-axis robot equipped with a granulate extrusion printing head; (b) the printed piece of a doubly curved composite shell with 1.2 m high and 24 cm wide; (c) outlook towards possible large-scale freeform printing [259].

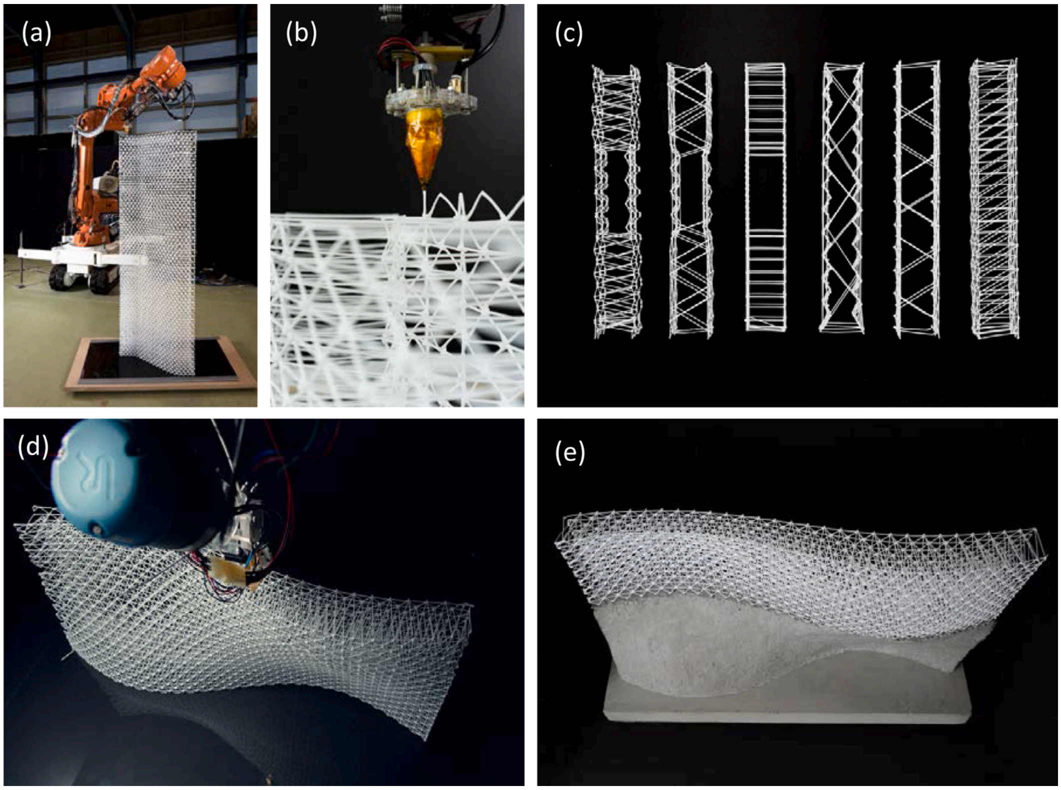

Fig. 21. Robotically fabricated spatial meshes based on FDM mechanism: ((a), (b) and (d)) different views of the movable robotic arm-assisted FDM printing of lattice mesh; (b) various meshes printed by the robot; (e) the printed ABS sample with sizes of approximately 80 × 60 × 8 cm was casted by concrete [261].

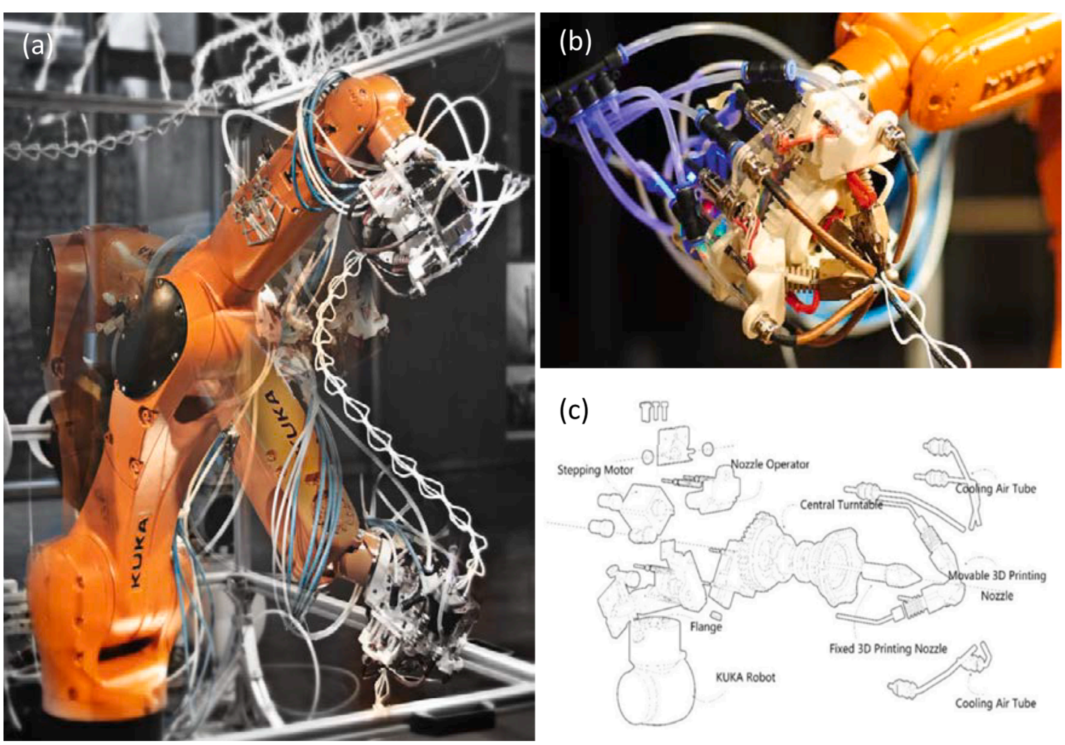

Fig. 22. Robotic multi-dimensional printing with structural performance: ((a) and (b)) the robot-assisted FDM printing process with multiple nozzles; (c) the exploded axonometric view of the mechanical system for the end effector [262].

Cartesian 3-axis planes [241,266]. Only two studies are published on the adoption of multi-axis robots to offer more DoF for tool heads in hybrid manufacturing. Keating and Oxman assembled a 6-axis robotic arm platform called compound fabrication where the major manufacturing methods including additive, formative and subtractive processes were combined. One case in this work was to add a milling effector and a urethane spraying head onto the robotic arm to cast a urethane part from a sculpted mold while the other case was to mount the build substrate onto the robot so that the work piece can be moved between the fixed ABS 3D printing head and milling head to manage the additive and subtractive processes [267]. By integrating an industrial robot arm with changeable FDM head and milling head, the hybrid manufacturing platform built by Li et al. supported the fabrication of freeform objects via non-linear trajectory movements. From the investigation of five case studies, this hybrid system exhibited numerous merits such as relatively low costs, short production time, minimized physical footprint, low collision probability and remarkable surface quality of parts [241]. Although the multi-axis robot engaged hybrid manufacturing technology provides higher adaptability and flexibility for multi-functional and multi-material part fabrication, the more complicated control system, process planning, computational simulation, hardware and kinematic configurations become the tremendous barrier to its progress.

7. Conclusions and future perspectives

After decades of research and development, FDM technology in the production of discontinuous fiber reinforced thermoplastic composites has experienced two stages of evolution: (1) the low-speed, small-scale fabrication of polymer composites via desktop 3D printers and HME-sourced filaments to realize high customization and extra properties from fiber fillers; (2) the high-speed, large-scale manufacturing of FRPC via the processing integration of FDM and HME into a single AM system with increased mass throughput and printing size. With the advancement of techniques in computing science, automatic manufacturing, process control and material science, we are now ushering in a new phase of developing multi-axis FDM strategies to break through the DoF limitation in conventional 3-axis printers and to achieve higher complexity and diversity in structure design, material option and product functionality. However, there are still numerous challenges needing to be conquered for the ultimate industrial application of this technology in fiber composite field:

- How to create a comprehensive methodology for optimizing fiber/matrix compositions to increase the versatility of composite printing
- How to enhance the interfacial adhesion between fibers and thermoplastic matrices both in HME and FDM so that inner-bead voids can be avoided
- How to identify an ideal compounding and extrusion process that can homogenize the fiber distribution and minimize the fiber damage for efficient stress transfer
- How to increase the printable fiber weight/volume fractions without causing surface defects in HME filament fabrication and nozzle clogging in FDM
- What is the influence of varying fiber specifications on the thermal and viscoelastic behaviours of melt flow, the resulting bond formation, dimensional stability and final print resolution
- How to fully eliminate the inter-bead and inter-layer voids with complete bond formation between adjacent beads
- How to expand the composite material bank applicable in the current large-scale FDM system that has very limited material options
- How to build a unified information flow for robot-assisted multi-axis printing so as to better link CAD, robotic arm and FDM processes that are based on different algorithms and languages
- How to improve the positioning of a robot manipulator in the FDM system so that higher printing accuracy can be achieved
- How to strike a balance between printing speed and resolution without compromising the overall quality of printed composites
- How to systematically integrate various in-situ monitoring and feedback units into HME and FDM systems so that the entire manufacturing chain can be regulated
- How to solve the increased complexity in the development of theoretical models and simulations for FDM composites due to the introduction of fibers
- How to maintain the repeatability and consistency for the FDM manufacturing of fiber/polymer composites with more process uncertainties
- How to establish the corresponding test standards for 3D printed FRPC that are still relied on conventional composite testing methods

Although we are still far from understanding the intricate relationship of all influencing parameters in the holistic FDM-FRPC system, the fast progress in this field has been witnessed especially in recent years. The fabrication of discontinuous fiber reinforced composites associated with the latest FDM techniques gives us a bright vision not only for the revolution of conventional composite manufacturing industries with high customization and full automation, but for the creation of some new fields that are still staying at theoretical study due to the production difficulty of their topologically intricate structures. Moreover, by leveraging the merits from this next generation of manufacturing, the incorporation of different fibers into the polymer matrix to print multi-fiber reinforced composites will need to grow for the development of advanced smart materials with multi-functionality. Moreover, as a branch of artificial intelligence, we believe machine learning [268] will also be a promising tool to probe the design space in FDM-FRPC system for the optimal fiber composite printing given its faster and smarter computing capacity compared to conventional modeling tools.

Declaration of Competing Interest

The authors declare that they have no known competing financial interests or personal relationships that could have appeared to influence the work reported in this paper.

References

[1] R.F. Gibson, A review of recent research on mechanics of multifunctional composite materials and structures, Compos. Struct. 92 (12) (2010) 2793–2810.
[2] V. Mittal, R. Saini, S. Sinha, Natural fiber-mediated epoxy composites–a review, Compos. B Eng. 99 (2016) 425–435.
[3] Q.H. Qin, J. Ye, Toughening mechanisms in composite materials, Elsevier, UK, 2015.
[4] H. Cen, Y. Kang, Z. Lei, Q.H. Qin, W. Qiu, Micromechanics analysis of Kevlar-29 aramid fiber and epoxy resin microdroplet composite by Micro-Raman spectroscopy, Compos. Struct. 75 (1) (2006) 532–538.
[5] S.-Y. Fu, X.-Q. Feng, B. Lauke, Y.-W. Mai, Effects of particle size, particle/matrix interface adhesion and particle loading on mechanical properties of particulate–polymer composites, Compos. Part B Eng. 39 (6) (2008) 933–961.
[6] R.F. Gibson, Principles of composite material mechanics, CRC press, 2016.
[7] Q.H. Qin, Q.S. Yang, Macro-micro theory on multifield coupling behavior of hetereogenous materials, Higher Education Press and Springer, Beijing, 2008.
[8] X.-Q. Feng, Y.-W. Mai, Q.H. Qin, A micromechanical model for interpenetrating multiphase composites, Comput. Mater. Sci. 28 (3) (2003) 486–493.
[9] M. Boopalan, M. Niranjanaa, M. Umapathy, Study on the mechanical properties and thermal properties of jute and banana fiber reinforced epoxy hybrid composites, Compos. Part B Eng. 51 (2013) 54–57.
[10] C. Hu, X. Liao, Q.-H. Qin, G. Wang, The fabrication and characterization of high density polyethylene composites reinforced by carbon nanotube coated carbon fibers, Compos. Part A Appl. Sci. Manuf. 121 (2019) 149–156.
[11] P. Parandoush, D. Lin, A review on additive manufacturing of polymer-fiber composites, Compos. Struct. 182 (2017) 36–53.
[12] L. Zhang, X. Wang, J. Pei, Y. Zhou, Review of automated fibre placement and its prospects for advanced composites, J. Mater. Sci. (2020) 1–35.
[13] R.L. Truby, J.A. Lewis, Printing soft matter in three dimensions, Nature 540 (7633) (2016) 371–378.
[14] R. Jiang, R. Kleer, F.T. Piller, Predicting the future of additive manufacturing: A Delphi study on economic and societal implications of 3D printing for 2030, Technol. Forecast. Soc. Chang. 117 (2017) 84–97.
[15] S.H. Huang, P. Liu, A. Mokasdar, L. Hou, Additive manufacturing and its societal impact: a literature review, Int. J. Adv. Manuf. Technol. 67 (5–8) (2013) 1191–1203.
[16] Y. Qin, Q. Qi, P.J. Scott, X. Jiang, Status, comparison, and future of the representations of additive manufacturing data, Comput. Aided Des. 111 (2019) 44–64.

[17] C.M. González-Henríquez, M.A. Sarabia-Vallejos, J. Rodriguez-Hernandez, Polymers for additive manufacturing and 4D-printing: Materials, methodologies, and biomedical applications, Prog. Polym. Sci. (2019).
[18] M. Attaran, The rise of 3-D printing: The advantages of additive manufacturing over traditional manufacturing, Bus. Horiz. 60 (5) (2017) 677–688.
[19] B. Sedacca, Hand built by lasers [additive layer manufacturing], Eng. Technol. 6 (1) (2011) 58–60.
[20] V. Dikshit, A.P. Nagalingam, Y.L. Yap, S.L. Sing, W.Y. Yeong, J. Wei, Investigation of quasi-static indentation response of inkjet printed sandwich structures under various indenter geometries, Materials 10 (3) (2017) 290.
[21] B. Berman, 3-D printing: The new industrial revolution, Bus. Horiz. 55 (2) (2012) 155–162.
[22] A. Bandyopadhyay, B. Heer, Additive manufacturing of multi-material structures, Mater. Sci. Eng.: R: Reports 129 (2018) 1–16.
[23] C.W. Hull, Apparatus for production of three-dimensional objects by stereolithography, United States Patent, Appl., No. 638905, Filed, 1984.
[24] A. Standard, Standard terminology for additive manufacturing technologies, ASTM International F2792–12a (2012).
[25] S.C. Ligon, R. Liska, J.r. Stampfl, M. Gurr, R. Mülhaupt, Polymers for 3D printing and customized additive manufacturing, Chemical reviews 117(15) (2017) 10212-10290.
[26] J.W. Stansbury, M.J. Idacavage, 3D printing with polymers: Challenges among expanding options and opportunities, Dent. Mater. 32 (1) (2016) 54–64.
[27] E. MacDonald, R. Wicker, Multiprocess 3D printing for increasing component functionality, Science 353 (6307) (2016) aaf2093.
[28] N. Saengchairat, T. Tran, C.-K. Chua, A review: Additive manufacturing for active electronic components, Virtual Phys. Prototyping 12 (1) (2017) 31–46.
[29] S. Bose, D. Ke, H. Sahasrabudhe, A. Bandyopadhyay, Additive manufacturing of biomaterials, Prog. Mater Sci. 93 (2018) 45–111.
[30] S. Lim, R.A. Buswell, T.T. Le, S.A. Austin, A.G. Gibb, T. Thorpe, Developments in construction-scale additive manufacturing processes, Autom. Constr. 21 (2012) 262–268.
[31] N. Guo, M.C. Leu, Additive manufacturing: technology, applications and research needs, Front. Mech. Eng. 8 (3) (2013) 215–243.
[32] H. Smith, GE aviation to grow better fuel nozzles using 3D printing, 3D Print. News Trends 17 (2013).
[33] J. Manyika, M. Chui, J. Bughin, R. Dobbs, P. Bisson, A. Marrs, Disruptive technologies: Advances that will transform life, business, and the global economy, McKinsey Global Institute San Francisco, CA, 2013.
[34] T.D. Ngo, A. Kashani, G. Imbalzano, K.T. Nguyen, D. Hui, Additive manufacturing (3D printing): A review of materials, methods, applications and challenges, Compos. Part B Eng. 143 (2018) 172–196.
[35] M. Araya-Calvo, I. López-Gómez, N. Chamberlain-Simon, J.L. León-Salazar, T. Guillén-Girón, J.S. Corrales-Cordero, O. Sánchez-Brenes, Evaluation of compressive and flexural properties of continuous fiber fabrication additive manufacturing technology, Addit. Manuf. 22 (2018) 157–164.
[36] B. Akhoundi, A.H. Behravesh, A. Bagheri Saed, Improving mechanical properties of continuous fiber-reinforced thermoplastic composites produced by FDM 3D printer, J. Reinf. Plast. Compos. 38 (3) (2019) 99–116.
[37] C. Kousiatza, D. Tzetzis, D. Karalekas, In-situ characterization of 3D printed continuous fiber reinforced composites: A methodological study using fiber Bragg grating sensors, Compos. Sci. Technol. 174 (2019) 134–141.
[38] R. Matsuzaki, T. Nakamura, K. Sugiyama, M. Ueda, A. Todoroki, Y. Hirano, Y. Yamagata, Effects of set curvature and fiber bundle size on the printed radius of curvature by a continuous carbon fiber composite 3D printer, Addit. Manuf. 24 (2018) 93–102.
[39] R. Matsuzaki, M. Ueda, M. Namiki, T.-K. Jeong, H. Asahara, K. Horiguchi, T. Nakamura, A. Todoroki, Y. Hirano, Three-dimensional printing of continuous-fiber composites by in-nozzle impregnation, Sci. Rep. 6 (2016) 23058.
[40] C. Hu, Q.H. Qin, H. Zhou, The design of an intermediate extrusion die for manufacturing continuous high performance fiber reinforced composite filaments, Australia, AU2019202860, 2019.
[41] G.T. Mark, A.S. Gozdz, Apparatus for fiber reinforced additive manufacturing, Google Patents (2017).
[42] C. Hu, Z. Sun, Y. Xiao, Q. Qin, Recent patents in additive manufacturing of continuous fiber reinforced composites, Recent Patents Mech. Eng. 12 (1) (2019) 25–36.
[43] A.N. Dickson, J.N. Barry, K.A. McDonnell, D.P. Dowling, Fabrication of continuous carbon, glass and Kevlar fibre reinforced polymer composites using additive manufacturing, Addit. Manuf. 16 (2017) 146–152.
[44] J. Vera-Sorroche, A. Kelly, E. Brown, P. Coates, N. Karnachi, E. Harkin-Jones, K. Li, J. Deng, Thermal optimisation of polymer extrusion using in-process monitoring techniques, Appl. Therm. Eng. 53 (2) (2013) 405–413.
[45] C. Abeykoon, Single screw extrusion control: A comprehensive review and directions for improvements, Control Eng. Pract. 51 (2016) 69–80.
[46] B. Claeys, A. Vervaeck, X.K. Hillewaere, S. Possemiers, L. Hansen, T. De Beer, J. P. Remon, C. Vervaet, Thermoplastic polyurethanes for the manufacturing of highly dosed oral sustained release matrices via hot melt extrusion and injection molding, Eur. J. Pharm. Biopharm. 90 (2015) 44–52.
[47] M.A. Repka, S. Shah, J. Lu, S. Maddineni, J. Morott, K. Patwardhan, N. N. Mohammed, Melt extrusion: process to product, Exp. Opin. Drug Deliv. 9 (1) (2012) 105–125.
[48] E.J. Siochi, D.C. Working, C. Park, P.T. Lillehei, J.H. Rouse, C.C. Topping, A. R. Bhattacharyya, S. Kumar, Melt processing of SWCNT-polyimide nanocomposite fibers, Compos. Part B Eng. 35 (5) (2004) 439–446.
[49] M. Sauceau, J. Fages, A. Common, C. Nikitine, E. Rodier, New challenges in polymer foaming: A review of extrusion processes assisted by supercritical carbon dioxide, Prog. Polym. Sci. 36 (6) (2011) 749–766.
[50] C. Abeykoon, Polymer extrusion: A study on thermal monitoring techniques and melting issues, Lap Lambert Academic Publishing (2012).
[51] C. Rauwendaal, Polymer extrusion, Carl Hanser Verlag GmbH Co KG, 2014.
[52] I. Aydin, F. Biglari, B. Briscoe, C. Lawrence, M. Adams, Physical and numerical modelling of ram extrusion of paste materials: conical die entry case, Comput. Mater. Sci. 18 (2) (2000) 141–155.
[53] H. Patil, R.V. Tiwari, M.A. Repka, Hot-melt extrusion: from theory to application in pharmaceutical formulation, Aaps Pharmscitech 17 (1) (2016) 20–42.
[54] A. Gaspar-Cunha, J.A. Covas, M.F.P. Costa, L. Costa, Optimization of single screw extrusion, 2018.
[55] S. Singhal, V.K. Lohar, V. Arora, Hot melt extrusion technique, 2011.
[56] R. Chokshi, H. Zia, Hot-melt extrusion technique: a review, 2004.
[57] M. Maniruzzaman, J.S. Boateng, M.J. Snowden, D. Douroumis, A review of hot-melt extrusion: process technology to pharmaceutical products, ISRN Pharmaceut. 2012 (2012).
[58] R. Censi, M.R. Gigliobianco, C. Casadidio, P. Di Martino, Hot melt extrusion: Highlighting physicochemical factors to be investigated while designing and optimizing a hot melt extrusion process, Pharmaceutics 10 (3) (2018) 89.
[59] M. Gale, Mixing in single screw extrusion, ISmithers, 2009.
[60] K. Wilczyński, A. Lewandowski, A. Nastaj, K. Wilczyński, Modeling for Starve Fed/Flood Fed Mixing Single-Screw Extruders, Int. Polym. Proc. 31 (1) (2016) 82–91.
[61] M.A. Repka, N. Langley, J. DiNunzio, Melt extrusion: materials, technology and drug product design, Springer Science & Business Media, 2013.
[62] K. Wilczyński, A. Nastaj, K. Wilczyński, Melting Model for Starve Fed Single Screw Extrusion of Thermoplastics, Int. Polym. Proc. 28 (1) (2013) 34–42.
[63] K. Wilczyński, A. Lewandowski, K.J. Wilczyński, Experimental study for starve-fed single screw extrusion of thermoplastics, Polym. Eng. Sci. 52 (6) (2012) 1258–1270.
[64] D.K. Tan, M. Maniruzzaman, A. Nokhodchi, Advanced pharmaceutical applications of hot-melt extrusion coupled with fused deposition modelling (FDM) 3D printing for personalised drug delivery, Pharmaceutics 10 (4) (2018) 203.
[65] K. Wilczynski, J.L. White, Melting model for intermeshing counter-rotating twin-screw extruders, Polym. Eng. Sci. 43 (10) (2003) 1715–1726.
[66] J.-M. Bouvier, O.H. Campanella, Extrusion processing technology: food and non-food biomaterials, John Wiley & Sons, 2014.
[67] Z. Tadmor, C.G. Gogos, Principles of polymer processing, John Wiley & Sons, 2013.
[68] M.M. Crowley, F. Zhang, M.A. Repka, S. Thumma, S.B. Upadhye, S. Kumar Battu, J.W. McGinity, C. Martin, Pharmaceutical applications of hot-melt extrusion: part I, Drug Dev. Ind. Pharm. 33 (9) (2007) 909–926.
[69] K. Wilczyński, A. Lewandowski, K.J. Wilczyński, Experimental study of melting of LDPE/PS polyblend in an intermeshing counter-rotating twin screw extruder, Polym. Eng. Sci. 52 (2) (2012) 449–458.
[70] M. Wilson, M.A. Williams, D.S. Jones, G.P. Andrews, Hot-melt extrusion technology and pharmaceutical application, Therapeutic Deliv. 3 (6) (2012) 787–797.
[71] W. Thiele, Twin-Screw Extrusion and Screw Design, CRC Press, Pharmaceutical Extrusion Technology, 2018, pp. 71–94.
[72] D.E. Crawford, Extrusion–back to the future: Using an established technique to reform automated chemical synthesis, Beilstein J. Org. Chem. 13 (1) (2017) 65–75.
[73] E. Uitterhaegen, Q.H. Nguyen, K. Sampaio, C. Stevens, O. Merah, T. Talou, L. Rigal, P. Evon, Extraction of coriander oil using twin-screw extrusion: Feasibility study and potential press cake applications, J. Am. Oil. Chem. Soc. 92 (8) (2015) 1219–1233.
[74] J. Thiry, F. Krier, B. Evrard, A review of pharmaceutical extrusion: Critical process parameters and scaling-up, Int. J. Pharm. 479 (1) (2015) 227–240.
[75] H.F. Giles Jr, E.M. Mount III, J.R. Wagner Jr., Extrusion: the definitive processing guide and handbook, William Andrew, 2004.
[76] J.M. Keen, C. Martin, A. Machado, H. Sandhu, J.W. McGinity, J.C. DiNunzio, Investigation of process temperature and screw speed on properties of a pharmaceutical solid dispersion using corotating and counter-rotating twin-screw extruders, J. Pharm. Pharmacol. 66 (2) (2014) 204–217.
[77] M. Spoerk, C. Savandaiah, F. Arbeiter, J. Sapkota, C. Holzer, Optimization of mechanical properties of glass-spheres-filled polypropylene composites for extrusion-based additive manufacturing, Polym. Compos. 40 (2) (2019) 638–651.
[78] A. Khudiakova, F. Arbeiter, M. Spoerk, M. Wolfahrt, D. Godec, G. Pinter, Inter-layer bonding characterisation between materials with different degrees of stiffness processed by fused filament fabrication, Addit. Manuf. 28 (2019) 184–193.
[79] F. Arbeiter, M. Spoerk, J. Wiener, A. Gosch, G. Pinter, Fracture mechanical characterization and lifetime estimation of near-homogeneous components produced by fused filament fabrication, Polym. Test. 66 (2018) 105–113.
[80] C. Hu, Q.H. Qin, W.N.J. Hau, H. Zhou, The twin-screw extrusion of long carbon fibre reinforced polylactic acid filaments for 3D printing, Australia, AU2019205991, 2019.
[81] M.M. Denn, Extrusion instabilities and wall slip, Annu. Rev. Fluid Mech. 33 (1) (2001) 265–287.
[82] S.S. Crump, Apparatus and method for creating three-dimensional objects, Google Patents (1992).

[83] B.N. Turner, S.A. Gold, A review of melt extrusion additive manufacturing processes: II. Materials, dimensional accuracy, and surface roughness, Rapid Prototyping J. (2015).

[84] N. van de Werken, H. Tekinalp, P. Khanbolouki, S. Ozcan, A. Williams, M. Tehrani, Additively manufactured carbon fiber-reinforced composites: State of the art and perspective, Addit. Manuf. 31 (2020), 100962.

[85] M.K. Agarwala, V.R. Jamalabad, N.A. Langrana, A. Safari, P.J. Whalen, S. C. Danforth, Structural quality of parts processed by fused deposition, Rapid Prototyp. J. (1996).

[86] J.M. Nasereddin, N. Wellner, M. Alhijjaj, P. Belton, S. Qi, Development of a simple mechanical screening method for predicting the feedability of a pharmaceutical FDM 3D printing filament, Pharm. Res. 35 (8) (2018) 151.

[87] A. Szmidt, A. Rębosz-Kurdek, New approaches of improving FDM/FFF printing technology, Mechanik 90 (3) (2017) 258–261.

[88] V.E. Kuznetsov, A.N. Solonin, O.D. Urzhumtsev, R. Schilling, A.G. Tavitov, Strength of PLA components fabricated with fused deposition technology using a desktop 3D printer as a function of geometrical parameters of the process, Polymers 10 (3) (2018) 313.

[89] T.N.A.T. Rahim, A.M. Abdullah, H. Md Akil, Recent developments in fused deposition modeling-based 3D printing of polymers and their composites, Polym. Rev. 59 (4) (2019) 589–624.

[90] C. Kim, D. Espalin, A. Cuaron, M.A. Perez, E. MacDonald, R.B. Wicker, A study to detect a material deposition status in fused deposition modeling technology, in: 2015 IEEE International Conference on Advanced Intelligent Mechatronics (AIM), IEEE, 2015, pp. 779-783.

[91] B.P. Heller, Effects of nozzle geometry and extrudate swell on fiber orientation in Fused Deposition Modeling nozzle flow, 2015.

[92] Y. Tlegenov, Y. San Wong, G.S. Hong, A dynamic model for nozzle clog monitoring in fused deposition modelling, Rapid Prototyp. J. (2017).

[93] H. Wu, Z. Yu, Y. Wang, Real-time FDM machine condition monitoring and diagnosis based on acoustic emission and hidden semi-Markov model, Int. J. Adv. Manuf. Technol. 90 (5–8) (2017) 2027–2036.

[94] Z. Yang, L. Jin, Y. Yan, Y. Mei, Filament breakage monitoring in fused deposition modeling using acoustic emission technique, Sensors 18 (3) (2018) 749.

[95] J. Go, S.N. Schiffres, A.G. Stevens, A.J. Hart, Rate limits of additive manufacturing by fused filament fabrication and guidelines for high-throughput system design, Addit. Manuf. 16 (2017) 1–11.

[96] J. Go, A.J. Hart, Fast desktop-scale extrusion additive manufacturing, Addit. Manuf. 18 (2017) 276–284.

[97] P. Kulkarni, A. Marsan, D. Dutta, A review of process planning techniques in layered manufacturing, Rapid Prototyp. J. (2000).

[98] F. Alabdullah, Fused deposition modeling (FDM) mechanism, Int. J. Sci. Eng. Res 7 (5) (2016).

[99] B.N. Turner, R. Strong, S.A. Gold, A review of melt extrusion additive manufacturing processes: I. Process design and modeling, Rapid Prototyp. J. (2014).

[100] S.-U. Zhang, J. Han, H.-W. Kang, Temperature-dependent mechanical properties of ABS parts fabricated by fused deposition modeling and vapor smoothing, Int. J. Precis. Eng. Manuf. 18 (5) (2017) 763–769.

[101] R. Jerez-Mesa, G. Gomez-Gras, J.A. Travieso-Rodriguez, V. Garcia-Plana, A comparative study of the thermal behavior of three different 3D printer liquefiers, Mechatronics 56 (2018) 297–305.

[102] A. Lanzotti, D.M. Del Giudice, A. Lepore, G. Staiano, M. Martorelli, On the geometric accuracy of RepRap open-source three-dimensional printer, J. Mech. Des. 137 (10) (2015).

[103] L. Brouwers, A. Teutelink, F.A. van Tilborg, M.A. de Jongh, K.W. Lansink, M. Bemelman, Validation study of 3D-printed anatomical models using 2 PLA printers for preoperative planning in trauma surgery, a human cadaver study, Eur. J. Trauma Emerg. Surg. 45 (6) (2019) 1013–1020.

[104] P. Chesser, B.K. Post, R. Lind, P. Lloyd, L.J. Love, Changing Print Resolution on BAAM Via Selectable Nozzles, Solid Freeform Fabricat. Symp. (2017).

[105] E.A. Papon, A. Haque, R.S. Ma, Effect of nozzle geometry on melt flow simulation and structural property of thermoplastic nanocomposites in fused deposition modeling, in: Proc. American society for composites, Thirty-second technical conference, 2017.

[106] H. Bikas, P. Stavropoulos, G. Chryssolouris, Additive manufacturing methods and modelling approaches: a critical review, Int. J. Adv. Manuf. Technol. 83 (1–4) (2016) 389–405.

[107] A. Pandey, S.K. Pradhan, Investigations into complete liquefier dynamics and optimization of process parameters for fused deposition modeling, Mater. Today:. Proc. 5 (5) (2018) 12940–12955.

[108] O. Günel, E. Koc, G. Tiryaki, Investigation of Heat Sink Geometry Effect on Cooling Performance for a FDM, 3D Printer Liquefier,, 2017.

[109] A. Bellini, S.u. Güçeri, M. Bertoldi, Liquefier dynamics in fused deposition, J. Manuf. Sci. Eng. 126(2) (2004) 237-246.

[110] H. Ramanath, C. Chua, K. Leong, K. Shah, Melt flow behaviour of poly-ε-caprolactone in fused deposition modelling, J. Mater. Sci. - Mater. Med. 19 (7) (2008) 2541–2550.

[111] M. AtifYardimci, T. Hattori, S.I. Guceri, S.C. Danforth, Thermal analysis of fused deposition, 1997 International Solid Freeform Fabrication Symposium (1997).

[112] R. Jerez-Mesa, J.A. Travieso-Rodriguez, X. Corbella, R. Busqué, G. Gómez-Gras, Finite element analysis of the thermal behavior of a RepRap 3D printer liquefier, Mechatronics 36 (2016) 119–126.

[113] J. Nixon, B. Dryer, I. Lempert, D. Bigio, Three parameter analysis of fiber orientation in fused deposition modeling geometries, in: Proc. of PPS conference, 2014.

[114] B.P. Heller, D.E. Smith, D.A. Jack, Effects of extrudate swell and nozzle geometry on fiber orientation in Fused Filament Fabrication nozzle flow, Addit. Manuf. 12 (2016) 252–264.

[115] J.R. Raney, B.G. Compton, J. Mueller, T.J. Ober, K. Shea, J.A. Lewis, Rotational 3D printing of damage-tolerant composites with programmable mechanics, Proc. Natl. Acad. Sci. 115 (6) (2018) 1198–1203.

[116] B. Brenken, E. Barocio, A. Favaloro, V. Kunc, R.B. Pipes, Fused filament fabrication of fiber-reinforced polymers: A review, Addit. Manuf. 21 (2018) 1–16.

[117] D. Pollard, C. Ward, G. Herrmann, J. Etches, Filament temperature dynamics in fused deposition modelling and outlook for control, Proc. Manuf. 11 (2017) 536–544.

[118] J.E. Seppala, S.H. Han, K.E. Hillgartner, C.S. Davis, K.B. Migler, Weld formation during material extrusion additive manufacturing, Soft Matter 13 (38) (2017) 6761–6769.

[119] D.A. Anderegg, H.A. Bryant, D.C. Ruffin, S.M. Skrip Jr, J.J. Fallon, E.L. Gilmer, M. J. Bortner, In-situ monitoring of polymer flow temperature and pressure in extrusion based additive manufacturing, Addit. Manuf. 26 (2019) 76–83.

[120] G. Goh, Y. Yap, H. Tan, S. Sing, G. Goh, W. Yeong, Process–structure–properties in polymer additive manufacturing via material extrusion: A review, Crit. Rev. Solid State Mater. Sci. 45 (2) (2020) 113–133.

[121] C. Bellehumeur, M. Bisaria, J. Vlachopoulos, An experimental study and model assessment of polymer sintering, Polym. Eng. Sci. 36 (17) (1996) 2198–2207.

[122] O. Pokluda, C.T. Bellehumeur, J. Vlachopoulos, Modification of Frenkel's model for sintering, AIChE J. 43 (12) (1997) 3253–3256.

[123] P.K. Gurrala, S.P. Regalla, Part strength evolution with bonding between filaments in fused deposition modelling: This paper studies how coalescence of filaments contributes to the strength of final FDM part, Virtual Phys. Prototyp. 9 (3) (2014) 141–149.

[124] Q. Sun, G. Rizvi, C. Bellehumeur, P. Gu, Effect of processing conditions on the bonding quality of FDM polymer filaments, Rapid Prototyp. J. (2008).

[125] C. Bellehumeur, L. Li, Q. Sun, P. Gu, Modeling of bond formation between polymer filaments in the fused deposition modeling process, J. Manuf. Processes 6 (2) (2004) 170–178.

[126] D. Bhalodi, K. Zalavadiya, P.K. Gurrala, Influence of temperature on polymer parts manufactured by fused deposition modeling process, J. Braz. Soc. Mech. Sci. Eng. 41 (3) (2019) 113.

[127] L. Li, Q. Sun, C. Bellehumeur, P. Gu, Investigation of bond formation in FDM process, Solid Freeform Fabricat. Proc. 403 (2002), 400407.

[128] A. Bellini, S. Güçeri, Mechanical characterization of parts fabricated using fused deposition modeling, Rapid Prototyp. J. (2003).

[129] J. Thomas, J. Rodríguez, Modeling the Fracture Strength between Fused-Deposition Extruded Roads, Int. Solid Freeform Fabricat. Symp. 16 (2000) 2000.

[130] M. Domingo-Espin, J.M. Puigoriol-Forcada, A.-A. Garcia-Granada, J. Llumà, S. Borros, G. Reyes, Mechanical property characterization and simulation of fused deposition modeling Polycarbonate parts, Mater. Des. 83 (2015) 670–677.

[131] H. Li, S. Zhang, Z. Yi, J. Li, A. Sun, J. Guo, G. Xu, Bonding quality and fracture analysis of polyamide 12 parts fabricated by fused deposition modeling, Rapid Prototyp. J. (2017).

[132] A.K. Ravi, A. Deshpande, K.H. Hsu, An in-process laser localized pre-deposition heating approach to inter-layer bond strengthening in extrusion based polymer additive manufacturing, J. Manuf. Processes 24 (2016) 179–185.

[133] J. Wang, H. Xie, Z. Weng, T. Senthil, L. Wu, A novel approach to improve mechanical properties of parts fabricated by fused deposition modeling, Mater. Des. 105 (2016) 152–159.

[134] J.F. Rodríguez, J.P. Thomas, J.E. Renaud, Mechanical behavior of acrylonitrile butadiene styrene (ABS) fused deposition materials. Experimental investigation, Rapid Prototyp. J. (2001).

[135] S. Costa, F. Duarte, J. Covas, Thermal conditions affecting heat transfer in FDM/FFE: a contribution towards the numerical modelling of the process: This paper investigates convection, conduction and radiation phenomena in the filament deposition process, Virtual Phys. Prototyp. 10 (1) (2015) 35–46.

[136] P.-H. Lee, H. Chung, S.W. Lee, J. Yoo, J. Ko, Dimensional accuracy in additive manufacturing processes, in: ASME 2014 International Manufacturing Science and Engineering Conference collocated with the JSME 2014 International Conference on Materials and Processing and the 42nd North American Manufacturing Research Conference, American Society of Mechanical Engineers Digital Collection, 2014.

[137] W. Wu, P. Geng, J. Zhao, Y. Zhang, D. Rosen, H. Zhang, Manufacture and thermal deformation analysis of semicrystalline polymer polyether ether ketone by 3D printing, Mater. Res. Innovat. 18(sup5) (2014) S5-12-S5-16.

[138] T.-M. Wang, J.-T. Xi, Y. Jin, A model research for prototype warp deformation in the FDM process, Int. J. Adv. Manuf. Technol. 33 (11–12) (2007) 1087–1096.

[139] Y. Zhang, K. Chou, A parametric study of part distortions in fused deposition modelling using three-dimensional finite element analysis, Proc. Inst. Mech. Eng., Part B: J. Eng. Manuf. 222 (8) (2008) 959–968.

[140] Y. Zhang, Y. Chou, Three-dimensional finite element analysis simulations of the fused deposition modelling process, Proc. Inst. Mech. Eng., Part B: J. Eng. Manuf. 220 (10) (2006) 1663–1671.

[141] A. Kantaros, D. Karalekas, Fiber Bragg grating based investigation of residual strains in ABS parts fabricated by fused deposition modeling process, Mater. Des. 50 (2013) 44–50.

[142] A. Armillotta, M. Bellotti, M. Cavallaro, Warpage of FDM parts: Experimental tests and analytic model, Rob. Comput. Integr. Manuf. 50 (2018) 140–152.

[143] O.A. Mohamed, S.H. Masood, J.L. Bhowmik, Experimental investigation of creep deformation of part processed by fused deposition modeling using definitive screening design, Addit. Manuf. 18 (2017) 164–170.

[144] T.W. Kerekes, H. Lim, W.Y. Joe, G.J. Yun, Characterization of process–deformation/damage property relationship of fused deposition modeling (FDM) 3D-printed specimens, Addit. Manuf. 25 (2019) 532–544.
[145] G. Alaimo, S. Marconi, L. Costato, F. Auricchio, Influence of meso-structure and chemical composition on FDM 3D-printed parts, Compos. B Eng. 113 (2017) 371–380.
[146] C. Theunissen, M. Kimpen, CHIMIA Report/Company News.
[147] S.-S. Yao, F.-L. Jin, K.Y. Rhee, D. Hui, S.-J. Park, Recent advances in carbon-fiber-reinforced thermoplastic composites: A review, Compos. B Eng. 142 (2018) 241–250.
[148] A.D. Valino, J.R.C. Dizon, A.H. Espera Jr, Q. Chen, J. Messman, R.C. Advincula, Advances in 3D printing of thermoplastic polymer composites and nanocomposites, Prog. Polym. Sci. 101162 (2019).
[149] I. Gibson, D.W. Rosen, B. Stucker, Additive manufacturing technologies, Springer, 2014.
[150] D. Bourell, J.P. Kruth, M. Leu, G. Levy, D. Rosen, A.M. Beese, A. Clare, Materials for additive manufacturing, CIRP Ann. 66 (2) (2017) 659–681.
[151] J. Frketic, T. Dickens, S. Ramakrishnan, Automated manufacturing and processing of fiber-reinforced polymer (FRP) composites: An additive review of contemporary and modern techniques for advanced materials manufacturing, Addit. Manuf. 14 (2017) 69–86.
[152] M. Spoerk, C. Holzer, J. Gonzalez-Gutierrez, Material extrusion-based additive manufacturing of polypropylene: A review on how to improve dimensional inaccuracy and warpage, J. Appl. Polym. Sci. 137 (12) (2020) 48545.
[153] S. Wojtyła, P. Klama, T. Baran, Is 3D printing safe? Analysis of the thermal treatment of thermoplastics: ABS, PLA, PET, and nylon, J. Occup. Environ. Hygiene 14 (6) (2017) D80–D85.
[154] M. Rinaldi, T. Ghidini, F. Cecchini, A. Brandao, F. Nanni, Additive layer manufacturing of poly (ether ether ketone) via FDM, Compos. B Eng. 145 (2018) 162–172.
[155] K.-J. Cheng, Y.-F. Liu, R. Wang, J.-X. Zhang, X.-F. Jiang, X.-T. Dong, X. Xu, Topological optimization of 3D printed bone analog with PEKK for surgical mandibular reconstruction, J. Mech. Behav. Biomed. Mater. 103758 (2020).
[156] M. Spoerk, F. Arbeiter, I. Raguž, G. Weingrill, T. Fischinger, G. Traxler, S. Schuschnigg, L. Cardon, C. Holzer, Polypropylene Filled With Glass Spheres in Extrusion-Based Additive Manufacturing: Effect of Filler Size and Printing Chamber Temperature, Macromol. Mater. Eng. 303 (7) (2018) 1800179.
[157] R. Zaldivar, D. Witkin, T. McLouth, D. Patel, K. Schmitt, J. Nokes, Influence of processing and orientation print effects on the mechanical and thermal behavior of 3D-Printed ULTEM® 9085 Material, Addit. Manuf. 13 (2017) 71–80.
[158] G. Cicala, G. Ognibene, S. Portuesi, I. Blanco, M. Rapisarda, E. Pergolizzi, G. Recca, Comparison of Ultem 9085 used in fused deposition modelling (FDM) with polytherimide blends, Materials 11 (2) (2018) 285.
[159] S. Gantenbein, K. Masania, W. Woigk, J.P. Sesseg, T.A. Tervoort, A.R. Studart, Three-dimensional printing of hierarchical liquid-crystal-polymer structures, Nature 561 (7722) (2018) 226–230.
[160] U. Kalsoom, P.N. Nesterenko, B. Paull, Recent developments in 3D printable composite materials, RSC Adv. 6 (65) (2016) 60355–60371.
[161] D. Depuydt, M. Balthazar, K. Hendrickx, W. Six, E. Ferraris, F. Desplentere, J. Ivens, A.W. Van Vuure, Production and characterization of bamboo and flax fiber reinforced polylactic acid filaments for fused deposition modeling (FDM), Polym. Compos. 40 (5) (2019) 1951–1963.
[162] V.K. Balla, K.H. Kate, J. Satyavolu, P. Singh, J.G.D. Tadimeti, Additive manufacturing of natural fiber reinforced polymer composites: Processing and prospects, Compos. Part B: Eng., 2019, 106956.
[163] A.G. Facca, M.T. Kortschot, N. Yan, Predicting the tensile strength of natural fibre reinforced thermoplastics, Compos. Sci. Technol. 67 (11–12) (2007) 2454–2466.
[164] D. Stoof, K. Pickering, Sustainable composite fused deposition modelling filament using recycled pre-consumer polypropylene, Compos. B Eng. 135 (2018) 110–118.
[165] G.D. Goh, Y.L. Yap, S. Agarwala, W.Y. Yeong, Recent progress in additive manufacturing of fiber reinforced polymer composite, Adv. Mater. Technol. 4 (1) (2019) 1800271.
[166] E.A. Papon, A. Haque, Fracture toughness of additively manufactured carbon fiber reinforced composites, Addit. Manuf. 26 (2019) 41–52.
[167] F. Ning, W. Cong, J. Qiu, J. Wei, S. Wang, Additive manufacturing of carbon fiber reinforced thermoplastic composites using fused deposition modeling, Compos. Part B Eng. 80 (2015) 369–378.
[168] M. Chapiro, Current achievements and future outlook for composites in 3D printing, Reinf. Plast. 60 (6) (2016) 372–375.
[169] R.T.L. Ferreira, I.C. Amatte, T.A. Dutra, D. Bürger, Experimental characterization and micrography of 3D printed PLA and PLA reinforced with short carbon fibers, Compos. Part B Eng. 124 (2017) 88–100.
[170] Y. Arao, S. Yumitori, H. Suzuki, T. Tanaka, K. Tanaka, T. Katayama, Mechanical properties of injection-molded carbon fiber/polypropylene composites hybridized with nanofillers, Compos. Part A Appl. Sci. Manuf. 55 (2013) 19–26.
[171] H.L. Tekinalp, V. Kunc, G.M. Velez-Garcia, C.E. Duty, L.J. Love, A.K. Naskar, C. A. Blue, S. Ozcan, Highly oriented carbon fiber–polymer composites via additive manufacturing, Compos. Sci. Technol. 105 (2014) 144–150.
[172] L.G. Blok, M.L. Longana, H. Yu, B.K. Woods, An investigation into 3D printing of fibre reinforced thermoplastic composites, Addit. Manuf. 22 (2018) 176–186.
[173] R.-M. Wang, S.-R. Zheng, Y.G. Zheng, Polymer matrix composites and technology, Elsevier, 2011.
[174] S. Mortazavian, A. Fatemi, Effects of fiber orientation and anisotropy on tensile strength and elastic modulus of short fiber reinforced polymer composites, Compos. Part B Eng. 72 (2015) 116–129.
[175] C. Duty, J. Failla, S. Kim, T. Smith, J. Lindahl, V. Kunc, Z-Pinning approach for 3D printing mechanically isotropic materials, Addit. Manuf. 27 (2019) 175–184.
[176] A. Le Duigou, M. Castro, R. Bevan, N. Martin, 3D printing of wood fibre biocomposites: From mechanical to actuation functionality, Mater. Des. 96 (2016) 106–114.
[177] G. Sodeifian, S. Ghaseminejad, A.A. Yousefi, Preparation of polypropylene/short glass fiber composite as Fused Deposition Modeling (FDM) filament, Results Phys. 12 (2019) 205–222.
[178] W. Zhong, F. Li, Z. Zhang, L. Song, Z. Li, Short fiber reinforced composites for fused deposition modeling, Mater. Sci. Eng., A 301 (2) (2001) 125–130.
[179] D. Filgueira, S. Holmen, J.K. Melbø, D. Moldes, A.T. Echtermeyer, G. Chinga-Carrasco, Enzymatic-assisted modification of thermomechanical pulp fibers to improve the interfacial adhesion with poly (lactic acid) for 3D printing, ACS Sustain. Chem. Eng. 5 (10) (2017) 9338–9346.
[180] J. Karger-Kocsis, H. Mahmood, A. Pegoretti, Recent advances in fiber/matrix interphase engineering for polymer composites, Prog. Mater Sci. 73 (2015) 1–43.
[181] S. Keszei, S. Matkó, G. Bertalan, P. Anna, G. Marosi, A. Toth, Progress in interface modifications: from compatibilization to adaptive and smart interphases, Eur. Polym. J. 41 (4) (2005) 697–705.
[182] F.R. Jones, Interphase in Fiber-Reinforced Composites, Wiley Encyclopedia of Composites (2011) 1–6.
[183] A.N. Netravali, K.L. Mittal, Fiber surface treatment: Relevance to interfacial characteristics, Wiley Encyclopedia of Composites (2011) 1–19.
[184] F. Ning, W. Cong, Y. Hu, H. Wang, Additive manufacturing of carbon fiber-reinforced plastic composites using fused deposition modeling: Effects of process parameters on tensile properties, J. Compos. Mater. 51 (4) (2017) 451–462.
[185] A. Anwer, H.E. Naguib, Multi-functional flexible carbon fiber composites with controlled fiber alignment using additive manufacturing, Addit. Manuf. 22 (2018) 360–367.
[186] D. Jiang, D.E. Smith, Anisotropic mechanical properties of oriented carbon fiber filled polymer composites produced with fused filament fabrication, Addit. Manuf. 18 (2017) 84–94.
[187] L.J. Love, V. Kunc, O. Rios, C.E. Duty, A.M. Elliott, B.K. Post, R.J. Smith, C. A. Blue, The importance of carbon fiber to polymer additive manufacturing, J. Mater. Res. 29 (17) (2014) 1893–1898.
[188] M. Shofner, F.J. Rodríguez-Macías, R. Vaidyanathan, E.V. Barrera, Single wall nanotube and vapor grown carbon fiber reinforced polymers processed by extrusion freeform fabrication, Compos. Part A: Appl. Sci. Manuf. 34(12) (2003) 1207-1217.
[189] M. Shofner, K. Lozano, F. Rodríguez-Macías, E. Barrera, Nanofiber-reinforced polymers prepared by fused deposition modeling, J. Appl. Polym. Sci. 89 (11) (2003) 3081–3090.
[190] W. Zhang, C. Cotton, J. Sun, D. Heider, B. Gu, B. Sun, T.-W. Chou, Interfacial bonding strength of short carbon fiber/acrylonitrile-butadiene-styrene composites fabricated by fused deposition modeling, Compos. Part B Eng. 137 (2018) 51–59.
[191] T. Hofstätter, I.W. Gutmann, T. Koch, D.B. Pedersen, G. Tosello, G. Heinz, H.N. Hansen, Distribution and orientation of carbon fibers in polylactic acid parts produced by fused deposition modeling, in: ASPE Summer Topical Meeting 2016, ASPE–The American Society for Precision Engineering, 2016.
[192] V. Kishore, X. Chen, C. Ajinjeru, A.A. Hassen, J.M. Lindahl, J. Failla, V. Kunc, C.E. Duty, Additive manufacturing of high performance semicrystalline thermoplastics and their composites, Oak Ridge National Lab.(ORNL), Oak Ridge, TN (United States), 2016.
[193] G. Liao, Z. Li, Y. Cheng, D. Xu, D. Zhu, S. Jiang, J. Guo, X. Chen, G. Xu, Y. Zhu, Properties of oriented carbon fiber/polyamide 12 composite parts fabricated by fused deposition modeling, Mater. Des. 139 (2018) 283–292.
[194] J. Naranjo-Lozada, H. Ahuett-Garza, P. Orta-Castañón, W.M. Verbeeten, D. Sáiz-González, Tensile properties and failure behavior of chopped and continuous carbon fiber composites produced by additive manufacturing, Addit. Manuf. 26 (2019) 227–241.
[195] O.S. Carneiro, A. Silva, R. Gomes, Fused deposition modeling with polypropylene, Mater. Des. 83 (2015) 768–776.
[196] R.W. Gray, D.G. Baird, J.H. Bøhn, Effects of processing conditions on short TLCP fiber reinforced FDM parts, Rapid Prototyp. J. (1998).
[197] A.R.T. Perez, D.A. Roberson, R.B. Wicker, Fracture surface analysis of 3D-printed tensile specimens of novel ABS-based materials, J. Fail. Anal. Prev. 14 (3) (2014) 343–353.
[198] F. Calignano, D. Manfredi, E.P. Ambrosio, S. Biamino, M. Lombardi, E. Atzeni, A. Salmi, P. Minetola, L. Iuliano, P. Fino, Overview on additive manufacturing technologies, Proc. IEEE 105 (4) (2017) 593–612.
[199] S.-H. Park, B.-K. Kang, J.E. Lee, S.W. Chun, K. Jang, Y.H. Kim, M.A. Jeong, Y. Kim, K. Kang, N.K. Lee, Design and fabrication of a thin-walled free-form scaffold on the basis of medical image data and a 3D printed template: its potential use in bile duct regeneration, ACS Appl. Mater. Interfaces 9 (14) (2017) 12290–12298.
[200] S.J. Park, J.E. Lee, J.H. Park, N.K. Lee, M.-Y. Lyu, K. Park, M.S. Koo, S.H. Cho, Y. Son, S.-H. Park, Enhanced solubility of the support in an FDM-based 3D printed structure using hydrogen peroxide under ultrasonication, Adv. Mater. Sci. Eng. 2018 (2018).
[201] E. Pei, C. Duran, V. Subbian, M.T. Giovanetti, J.R. Simkins, F.R. Beyette Jr, Experimental desktop 3D printing using dual extrusion and water-soluble polyvinyl alcohol, Rapid Prototyp. J. (2015).
[202] C.C. Kuo, Y.C. Tsou, B.C. Chen, Enhancing the efficiency of removing support material from rapid prototype parts, Materialwiss. Werkstofftech. 43 (3) (2012) 234–240.

[203] C.E. Duty, V. Kunc, B. Compton, B. Post, D. Erdman, R. Smith, R. Lind, P. Lloyd, L. Love, Structure and mechanical behavior of Big Area Additive Manufacturing (BAAM) materials, Rapid Prototyp. J. (2017).
[204] L.J. Love, C. Duty, Cincinnati Big Area Additive Manufacturing, BAAM), Oak Ridge, TN, 2015.
[205] A.A. Hassen, R. Springfield, J. Lindahl, B. Post, L. Love, C. Duty, U. Vaidya, R. B. Pipes, V. Kunc, The durability of large-scale additive manufacturing composite molds, CAMX 2016 (2016) 26–29.
[206] P. Geng, J. Zhao, W. Wu, Y. Wang, B. Wang, S. Wang, G. Li, Effect of Thermal Processing and Heat Treatment Condition on 3D Printing PPS Properties, Polymers 10 (8) (2018) 875.
[207] E. Barocio, B. Brenken, A. Favaloro, J. Ramirez, V. Kunc, R.B. Pipes, Fusion bonding simulations of semi-crystalline polymer composites in the extrusion deposition additive manufacturing process, Proceedings of the American Society for Composites—Thirty-second Technical Conference (2017).
[208] N.M. DeNardo, Additive manufacturing of carbon fiber-reinforced thermoplastic composites, 2016.
[209] CINCINNATI, CIBAAM 3D Printed Projects, 2018. https://www.e-ci.com/baam-3dprinted-projects/.
[210] B. Post, P.D. Lloyd, J. Lindahl, R.F. Lind, L.J. Love, V. Kunc, The economics of big area additive manufacturing, in: Proceedings of the 27th Annual International Solid Freeform Fabrication Symposium, 2016, pp. 8–10.
[211] C. Hill, R. Bedsole, K. Rowe, C. Duty, C. Ajinjeru, V. Kunc, D. Riha, Big Area Additive Manufacturing (BAAM) Materials Development and Reinforcement with Advanced Composites, Inst. for Advanced Composites Manufacturing Innovation (IACMI), Knoxville …, 2018.
[212] Z. Tao, Q. Guo, X. Gao, L. Liu, Graphite fiber/copper composites with near-zero thermal expansion, Mater. Des. 33 (2012) 372–375.
[213] P.K. Rao, Z. Kong, C.E. Duty, R.J. Smith, V. Kunc, L.J. Love, Assessment of dimensional integrity and spatial defect localization in additive manufacturing using spectral graph theory, J. Manuf. Sci. Eng. 138 (5) (2016).
[214] E. Barocio, B. Brenken, A. Favaloro, M. Ramirez, J. Ramirez, R.B. Pipes, Prediction of the degree of bonding in the extrusion deposition additive manufacturing process of semi-crystalline polymer composites, in: Proceedings of the Dassault Systemes' Science in the Age of Experience, 2018, pp. 18–21.
[215] T.Z. Sudbury, R. Springfield, V. Kunc, C. Duty, An assessment of additive manufactured molds for hand-laid fiber reinforced composites, Int. J. Adv. Manuf. Technol. 90 (5–8) (2017) 1659–1664.
[216] V. Kunc, J. Lindahl, R. Dinwiddie, B. Post, L. Love, M. Matlack, R. Fahey, A. Hassen, Investigation of in-autoclave additive manufacturing composite tooling, CAMX Conference (2016).
[217] E. Barocio, B. Brenken, A. Favaloro, R. Pipes, Extrusion deposition additive manufacturing of composite molds for high-temperature applications, in: Proceedings of the Int. SAMPE Tech. Conf., Seattle, WA, USA, 2017, pp. 22-25.
[218] C.E. Duty, T. Drye, A. Franc, Material development for tooling applications using big area additive manufacturing (BAAM), Oak Ridge National Lab.(ORNL), Oak Ridge, TN (United States). Manufacturing …, 2015.
[219] V. Kishore, C. Ajinjeru, A. Nycz, B. Post, J. Lindahl, V. Kunc, C. Duty, Infrared preheating to improve interlayer strength of big area additive manufacturing (BAAM) components, Addit. Manuf. 14 (2017) 7–12.
[220] B.G. Compton, B.K. Post, C.E. Duty, L. Love, V. Kunc, Thermal analysis of additive manufacturing of large-scale thermoplastic polymer composites, Addit. Manuf. 17 (2017) 77–86.
[221] L.J. Love, Utility of big area additive manufacturing (BAAM) for the rapid manufacture of customized electric vehicles, Oak Ridge National Lab.(ORNL), Oak Ridge, TN (United States). Manufacturing …, 2015.
[222] C. Ajinjeru, V. Kishore, Z. Sudbury, J. Lindahl, A. Hassen, B. Post, L. Love, V. Kunc, C. Duty, The Influence of Rheology on Melt Processing Conditions of Carbon Fiber Reinforced Polyetherimide for Big Area Additive Manufacturing (BAAM), in: SAMPE Conference Proceedings. Seattle WA, 2017.
[223] Q.H. Qin, Hybrid Trefftz finite-element approach for plate bending on an elastic foundation, Appl. Math. Model. 18 (6) (1994) 334–339.
[224] Q.H. Qin, Y.-W. Mai, S.-W. Yu, Effective moduli for thermopiezoelectric materials with microcracks, Int. J. Fract. 91 (4) (1998) 359–371.
[225] J. Jirousek, Q.H. Qin, Application of hybrid-Trefftz element approach to transient heat conduction analysis, Comput. Struct. 58 (1) (1996) 195–201.
[226] Q.H. Qin, Hybrid-Trefftz finite element method for Reissner plates on an elastic foundation, Comput. Methods Appl. Mech. Eng. 122 (3–4) (1995) 379–392.
[227] H. Wang, Q.H. Qin, Hybrid FEM with fundamental solutions as trial functions for heat conduction simulation, Acta Mech. Solida Sin. 22 (5) (2009) 487–498.
[228] M. Talagani, S. DorMohammadi, R. Dutton, C. Godines, H. Baid, F. Abdi, V. Kunc, B. Compton, S. Simunovic, C. Duty, Numerical simulation of big area additive manufacturing (3D printing) of a full size car, SAMPE J. 51 (4) (2015) 27–36.
[229] B. Brenken, E. Barocio, A. Favaloro, V. Kunc, R.B. Pipes, Development and validation of extrusion deposition additive manufacturing process simulations, Addit. Manuf. 25 (2019) 218–226.
[230] S.W. Williams, F. Martina, A.C. Addison, J. Ding, G. Pardal, P. Colegrove, Wire+arc additive manufacturing, Mater. Sci. Technol. 32 (7) (2016) 641–647.
[231] K.-M.M. Tam, C.T. Mueller, Additive manufacturing along principal stress lines, 3D Print. Addit. Manuf. 4 (2) (2017) 63–81.
[232] K.-M.M. Tam, D.J. Marshall, M. Gu, J. Kim, Y. Huang, J. Lavallee, C.T. Mueller, Fabrication-aware structural optimisation of lattice additive-manufactured with robot-arm, Int. J. Rapid Manuf. 7 (2–3) (2018) 120–168.
[233] X. Wu, Y. Su, J. Shi, Perspective of additive manufacturing for metamaterials development, Smart Mater. Struct. 28 (9) (2019), 093001.
[234] R.S. Lakes, Negative-Poisson's-ratio materials: auxetic solids, Annu. Rev. Mater. Res. 47 (2017) 63–81.
[235] U.R. Gabinet, C.O. Osuji, Optical materials and metamaterials from nanostructured soft matter, Nano Res. (2019) 1–12.
[236] J.U. Surjadi, L. Gao, H. Du, X. Li, X. Xiong, N.X. Fang, Y. Lu, Mechanical metamaterials and their engineering applications, Adv. Eng. Mater. 21 (3) (2019) 1800864.
[237] G. Dong, G. Wijaya, Y. Tang, Y.F. Zhao, Optimizing process parameters of fused deposition modeling by Taguchi method for the fabrication of lattice structures, Addit. Manuf. 19 (2018) 62–72.
[238] A.V. Shembekar, Y.J. Yoon, A. Kanyuck, S.K. Gupta, Trajectory planning for conformal 3d printing using non-planar layers, ASME 2018 International Design Engineering Technical Conferences and Computers and Information in Engineering Conference, American Society of Mechanical Engineers Digital Collection (2018).
[239] I. Ishak, J. Fisher, P. Larochelle, Robot arm platform for additive manufacturing: Multi-plane printing, in: Proceedings of the 2016 Florida Conference on Recent Advances in Robotics (FCRAR 2016), 2016.
[240] F. Wulle, D. Coupek, F. Schäffner, A. Verl, F. Oberhofer, T. Maier, Workpiece and machine design in additive manufacturing for multi-axis fused deposition modeling, Proc. CIRP 60 (2017) 229–234.
[241] L. Li, A. Haghighi, Y. Yang, A novel 6-axis hybrid additive-subtractive manufacturing process: Design and case studies, J. Manuf. Processes 33 (2018) 150–160.
[242] W. Gao, Y. Zhang, D.C. Nazzetta, K. Ramani, R.J. Cipra, RevoMaker: Enabling multi-directional and functionally-embedded 3D printing using a rotational cuboidal platform, in: Proceedings of the 28th Annual ACM Symposium on User Interface Software & Technology, 2015, pp. 437-446.
[243] R. Wu, H. Peng, F. Guimbretière, S. Marschner, Printing arbitrary meshes with a 5DOF wireframe printer, ACM Trans. Graph. (TOG) 35 (4) (2016) 1–9.
[244] X. Song, Y. Pan, Y. Chen, Development of a low-cost parallel kinematic machine for multidirectional additive manufacturing, J. Manuf. Sci. Eng. 137 (2) (2015).
[245] D. Gan, J.S. Dai, J. Dias, R. Umer, L. Seneviratne, Singularity-free workspace aimed optimal design of a 2T2R parallel mechanism for automated fiber placement, J. Mech. Robot. 7 (4) (2015).
[246] A. Rastegarpanah, M. Saadat, A. Borboni, Parallel robot for lower limb rehabilitation exercises, Appl. Bionics Biomech. 2016 (2016).
[247] M. Vallés, P. Araujo-Gómez, V. Mata, A. Valera, M. Díaz-Rodríguez, Á. Page, N. M. Farhat, Mechatronic design, experimental setup, and control architecture design of a novel 4 DoF parallel manipulator, Mech. Based Des. Struct. Mach. 46 (4) (2018) 425–439.
[248] M.J. Saracen, A.W. Carrano, T.D. Henderson, Robotic arm for patient positioning assembly, Google Patents (2012).
[249] I. Bin Ishak, J. Fisher, P. Larochelle, Robot arm platform for additive manufacturing using multi-plane toolpaths, in: ASME 2016 International Design Engineering Technical Conferences and Computers and Information in Engineering Conference, American Society of Mechanical Engineers Digital Collection, 2016.
[250] B. Khoshnevis, Automated construction by contour crafting—related robotics and information technologies, Autom. Constr. 13 (1) (2004) 5–19.
[251] G.Q. Zhang, X. Li, R. Boca, J. Newkirk, B. Zhang, T.A. Fuhlbrigge, H.K. Feng, N.J. Hunt, Use of industrial robots in additive manufacturing-a survey and feasibility study, in: ISR/Robotik 2014; 41st International Symposium on Robotics, VDE, 2014, pp. 1-6.
[252] M. Pollák, J. Török, J. Zajac, M. Kočiško, M. Telišková, The structural design of 3D print head and execution of printing via the robotic arm ABB IRB 140, in: 2018 5th International Conference on Industrial Engineering and Applications (ICIEA), IEEE, 2018, pp. 194-198.
[253] A. Dine, G.-C. Vosniakos, On the development of a robot-operated 3D-printer, Proc. Manuf. 17 (2018) 6–13.
[254] B.J. Brooks, K.M. Arif, S. Dirven, J. Potgieter, Robot-assisted 3D printing of biopolymer thin shells, Int. J. Adv. Manuf. Technol. 89 (1–4) (2017) 957–968.
[255] K. Ma, T. Zhao, L. Yang, P. Wang, J. Jin, H. Teng, D. Xia, L. Zhu, L. Li, Q. Jiang, Application of robotic-assisted in situ 3D printing in cartilage regeneration with HAMA hydrogel: An in vivo study, J. Adv. Res. 23 (2020) 123–132.
[256] C. Wu, C. Dai, G. Fang, Y.-J. Liu, C.C. Wang, RoboFDM: A robotic system for support-free fabrication using FDM, in: 2017 IEEE International Conference on Robotics and Automation (ICRA), IEEE, 2017, pp. 1175-1180.
[257] I.B. Ishak, P. Larochelle, MotoMaker: a robot FDM platform for multi-plane and 3D lattice structure printing, Mech. Based Des. Struct. Mach. 47 (6) (2019) 703–720.
[258] W. McGee, K. Velikov, G. Thun, D. Tish, Infundibuliforms: kinetic systems, additive manufacturing for cable nets and tensile surface control, Rethinking Design and Construction, Fabricate, 2017, pp. 4–6.
[259] B. Felbrich, F. Wulle, C. Allgaier, A. Menges, A. Verl, K. Wurst, J. Nebelsick, A novel rapid additive manufacturing concept for architectural composite shell construction inspired by the shell formation in land snails, Bioinspirat. Biomimet. 13 (2) (2018), 026010.
[260] N.P. Hack, W.V. Lauer, F.M. Gramazio, M. Kohler, N. Blank, Method of fabricating a 3-dimensional structure, mesh formwork element for fabricating a 3-dimensional structure and method of fabricating the same, Google Patents (2020).
[261] N. Hack, W.V. Lauer, Mesh-Mould: Robotically Fabricated Spatial Meshes as Reinforced Concrete Formwork, Architect. Des. 84 (3) (2014) 44–53.
[262] P.F. Yuan, H. Meng, L. Yu, L. Zhang, Robotic multi-dimensional printing based on structural performance, Robotic Fabrication in Architecture, Art and Design, Springer 2016 (2016) 92–105.

[263] Z. Zhu, V.G. Dhokia, A. Nassehi, S.T. Newman, A review of hybrid manufacturing processes–state of the art and future perspectives, Int. J. Comput. Integr. Manuf. 26 (7) (2013) 596–615.
[264] S.T. Newman, Z. Zhu, V. Dhokia, A. Shokrani, Process planning for additive and subtractive manufacturing technologies, CIRP Ann. 64 (1) (2015) 467–470.
[265] D. Aspinwall, R. Dewes, J. Burrows, M. Paul, B. Davies, Hybrid high speed machining (HSM): system design and experimental results for grinding/HSM and EDM/HSM, CIRP Ann. 50 (1) (2001) 145–148.
[266] W.-C. Lee, C.-C. Wei, S.-C. Chung, Development of a hybrid rapid prototyping system using low-cost fused deposition modeling and five-axis machining, J. Mater. Process. Technol. 214 (11) (2014) 2366–2374.
[267] S. Keating, N. Oxman, Compound fabrication: A multi-functional robotic platform for digital design and fabrication, Rob. Comput. Integr. Manuf. 29 (6) (2013) 439–448.
[268] J. Dong, Q.H. Qin, Y. Xiao, Nelder-Mead optimization of elastic metamaterials via machine-learning-aided surrogate modelling, Int. J. Appl. Mech. 12 (1) (2020) 2050011.